Electrochemical Control for Corrosion in Molten Chlorides During CSP Plant Operation

Kerry C. Rippy

National Renewable Energy Laboratory

NREL is a national laboratory of the U.S. Department of Energy
Office of Energy Efficiency & Renewable Energy
Operated by the Alliance for Sustainable Energy, LLC

This report is available at no cost from the National Renewable Energy Laboratory (NREL) at www.nrel.gov/publications.

Contract No. DE-AC36-08GO28308

Technical Report
NREL/TP-5500-85796
April 2024

Electrochemical Control for Corrosion in Molten Chlorides During CSP Plant Operation

Kerry C. Rippy

National Renewable Energy Laboratory

Suggested Citation
Rippy, Kerry C. 2024. *Electrochemical Control for Corrosion in Molten Chlorides During CSP Plant Operation*. Golden, CO: National Renewable Energy Laboratory. NREL/TP-5500-85796. https://www.nrel.gov/docs/fy24osti/85796.pdf.

NREL is a national laboratory of the U.S. Department of Energy
Office of Energy Efficiency & Renewable Energy
Operated by the Alliance for Sustainable Energy, LLC

This report is available at no cost from the National Renewable Energy Laboratory (NREL) at www.nrel.gov/publications.

Contract No. DE-AC36-08GO28308

Technical Report
NREL/TP-5500-85796
April 2024

National Renewable Energy Laboratory
15013 Denver West Parkway
Golden, CO 80401
303-275-3000 • www.nrel.gov

NOTICE

This work was authored by the National Renewable Energy Laboratory, operated by Alliance for Sustainable Energy, LLC, for the U.S. Department of Energy (DOE) under Contract No. DE-AC36-08GO28308. Funding provided by the U.S. Department of Energy Office of Energy Efficiency and Renewable Energy Solar Energy Technologies Office. The views expressed herein do not necessarily represent the views of the DOE or the U.S. Government.

This report is available at no cost from the National Renewable Energy Laboratory (NREL) at www.nrel.gov/publications.

U.S. Department of Energy (DOE) reports produced after 1991 and a growing number of pre-1991 documents are available free via www.OSTI.gov.

Cover Photos by Dennis Schroeder: (clockwise, left to right) NREL 51934, NREL 45897, NREL 42160, NREL 45891, NREL 48097, NREL 46526.

NREL prints on paper that contains recycled content.

Final Report

Project Title:	Electrochemical Control for Corrosion in Molten Chlorides During CSP Plant Operation
Project Period:	01/10/20 – 12/31/22
Project Budget:	$1,125,708
Submission Date:	2/01/23
Recipient:	National Renewable Energy Laboratory (NREL)
Address:	15013 Denver West Parkway Golden, CO 80401-3305
Award Number:	DE-EE00035931
Principal Investigator:	Dr. Kerry C. Rippy Phone: +1 (970) 274-6017 Email: Kerry.Rippy@nrel.gov
Business Contact:	Craig Turchi Phone: +1 (303) 384-7565 Email: craig.turchi@nrel.gov
Technology Manager:	Shane Powers
Project Officer:	Christine Bing

Agency to which Report is Submitted:	DOE/EERE Solar Technologies Office	
FOA Name:		
FOA Number:	DE-LC-000L044	
Report:	Final Scientific/Technical Report	
Award Type:	Cooperative Agreement	
Award Number:	DE-EE00035931	
Prime Recipient:	National Renewable Energy Laboratory (NREL)	
Prime Recipient Type:	National Lab, For-Profit, Non-Profit, University	
Project Title:	Electrochemical Control for Corrosion in Molten Chlorides During CSP Plant Operation	
Principal Investigator (PI):	Dr. Kerry C. Rippy; Researcher III – Chemistry; Kerry.Rippy@nrel.gov; +1 (970) 274-6017	
DOE Technology Manager (TM):	Shane Powers	
DOE Technical Project Officer (TPO):	Christine Bing	
Prime Recipient DUNS Number:	805948051 + 0000	
Award Period of Performance (POP):	Start: 01/10/2020	End: 12/31/2022
Award Budget Period (BP):	Start: /XX/XXXX	End: 12/31/2022
Date of Report:	02/01/2023	
Reporting Period (covered by this report):	01/10/2020 to 12/31/2022	

Acknowledgement: **“**This material is based upon work supported by the Department of Energy, Office of Energy Efficiency and Renewable Energy, Solar Energy Technologies Office, Tech to Market Sub-program, under Award Number DE-EE00035931.

Executive Summary:

The Liquid Pathway of the Concentrating Solar Power Generation 3 (CSP Gen3) program proposed low-cost molten chloride salt for energy storage. However, online corrosion control was identified as a remining major risk of the Liquid Pathway approach. This project addressed that risk. Electrochemical solutions for corrosion mitigation during CSP plant operation were investigated and their feasibility and scalability were evaluated.

The leading cause of corrosion in molten chloride salt systems was identified as corrosive impurities that form within the salt upon exposure to trace amounts of air and moisture. Leveraging electrochemistry, reduction/oxidation reactions can be employed to remove these corrosive impurities.

In Phase 1 of this project, a bench-scale batch electrochemical reactor was designed, fabricated, and used to assess the kinetics and thermodynamics of electrochemical salt purification. In Phase 2, a laboratory-scale flow reactor was designed, fabricated, and used to assess the efficacy of the electrochemical method under flowing conditions. Results show that under proposed operating conditions for the Liquid Pathway Gen3 Pilot Plant, the electrochemical method is significantly more effective at removing impurities than alternative chemical and thermal methods, and that the electrochemical method produces less harmful byproducts.

A key advance made during this project was the development of a 2-electrode method for electrochemical purification that is more scalable than previously developed 3-electrode methods. This novel method is based on Magnesium (Mg) electrowinning. A provisional patent based on this invention has been submitted (USPTO Application No. 63/480,355).

Additional key advances made during this project include assessment of the effect of dissimilar alloys on corrosion, kinetic and thermodynamic evaluation of thermolysis reactions of impurities within the molten salt, characterization of byproducts of purification reactions, and generation of IP focused on isolating value-added products using molten salt-based electrochemistry that could be deployed to valorize the process (USPTO Application No. 63/478,806).

Ultimately, this project represented a step toward feasibility of Liquid Pathway Gen3 CSP. The proposed method would significantly reduce capital expenses and operating costs and increase plant profitability by enabling the use of less expensive alloys, decreasing maintenance, and increasing plant longevity.

Key focus areas for follow-on work have been identified as 1) evaluation of the efficacy of the electrochemical method under turbulent conditions in a larger flow system, such as the FASTR loop, 2) development of methods for removal of purification byproducts, 3) modeling pilot and industrial scale performance of electrochemical salt purification during plant operation and 4) further assessment of the effect of impurities on salt vapor phase.

Table of Contents

1. Background:

The Liquid Pathway of the Concentrating Solar Power Generation 3 (CSP Gen3) has selected a NaCl-KCl-$MgCl_2$ ternary chloride salt for use as a thermal energy storage fluid.[1, 2] However, online corrosion control was identified as a remining major risk of the Liquid Pathway approach.[3-5] Therefore, the primary objective of this project is to develop an electrochemical corrosion control system for molten chloride salts suitable for use during CSP plant operation.

Impurity control in Mg based chloride salts has been well established due to its industrial application in Mg electrowinning.[6] In Mg electrowinning cells the purity of the salt affects the Faradaic efficiency of the unit and the rate of the graphite anode consumption. Typical strategies involve a slow heating step to remove residual moisture under a chlorinating environment to avoid formation of MgOHCl and MgO. Slow heating is crucial to avoid the formation of MgOHCl, which has been found to decompose at temperatures above 550 °C.[1, 7, 8] Zhao et al. improved upon this process by adding elemental Mg during the purification process and showed MgOHCl concentrations of ~1000 ppm after the purification protocol.[1] This process is incorporated into the Liquid Pathways' envisioned Gen3 CSP plant as a pre-purification step.[4] However, it is not an effective solution for purification of salt during plant operation, as cold-side temperatures of Gen3 CSP plants (500 ºC) are below the temperature for which this method is effective.

Therefore, an electrochemical corrosion control system is proposed based on a 3-electrode method described in the literature.[7, 9-17] An anode, a cathode, and a reference electrode are employed. In this electrochemical method, bulk electropositive metal electrodes and electrical energy increase the dissolution kinetics of the active metals into the molten chloride, overcoming the problems associated with operating temperatures below the active metallic Mg melting point. Under these conditions, the following reactions have been proposed:

$2MgOHCl \rightarrow 2MgOH^+ + 2Cl^-$	[*molten salt*]	[1-1]
$Mg^{2+} + 2Cl^- \rightarrow MgCl_2$	[*molten salt*]	[1-2]
$2MgOH^+ + 2e^- \rightarrow 2MgO + H_2(g)$	[*cathode*]	[1-3]
$Mg(s) \rightarrow Mg^{2+} + 2e^-$	[*anode*]	[1-4]
$2MgOHCl + Mg(s) \rightarrow MgCl_2 + 2MgO + H_2(g)$	[*overall reaction*]	[1-5]

It was hypothesized that this electrochemical control process could be scaled up to a commercially viable system. The rates of electrode reactions [1-3] and [1-4] are expected to be high and easy to control quickly at low voltages, so targeted elimination of corrosive impurities will be feasible immediately after oxygen and moisture ingresses are detected. At the electrochemical cell, corrosive impurities will be eliminated instantly through a redox-control mechanism. At the cathode, the formation of insoluble MgO will be managed to physically separate this particulate byproduct.

In Phase 1 of this project, a batch scale reactor was proposed to remove impurities using this electrochemical technique. Modeling was used to show how such a system could be scaled up and applied to a flowing system, which was built and evaluated in Phase 2. Furthermore, galvanic corrosion, which is a concern in metallic systems containing dissimilar components exposed to molten salt, was evaluated.

2. Project Objectives:

This project will accelerate national goals of clean energy by increasing feasibility, reliability, and durability of molten chloride salt-based thermal energy systems, and by decreasing capital costs by enabling use of less expensive alloys in these systems. While methods for pre-purification of chloride salts have been developed to ensure no corrosive impurities are present upon Gen3 CSP plant start-up[1, 18], the proposed work is the first corrosion mitigation solution that could be deployed continuously *during operation* of a Gen3 CSP plant. Ingress of a small amount of moisture and water during plant operation is inevitable.[4] Thus, corrosive impurities will form during plant operation, making the proposed solution essential.[1, 15, 19, 20] Development of the proposed electrochemical solution proceeds via the tasks outlined in Table 2-1.

Table 2-1. *Project Tasks*

Task #	Task Name and Description
1	**Task Name:** Electrochemical minimization of corrosive impurities **Task Description:** Electrochemical minimization of corrosive impurities at the low temperature point as might be envisioned in a Gen3 CSP facility.
2	**Task Name:** Galvanic corrosion assessment **Task Description:** Galvanic corrosion control at the low and high temperature points as might be envisioned in a Gen3 CSP facility.
3	**Task Name:** Removal of cathodic MgO produced **Task Description:** Effective removal and collection of cathodic impurity build-up.
4	**Task Name:** Conceptual/preliminary engineering design of an electrochemical purification cell **Task Description:** Provide a conceptual/preliminary engineering design of an electrochemical cell for purification of molten chlorides for the low temperature point as might be envisioned in a Gen3 CSP facility. The design will target the support to a 2MWth molten chloride flow loop.
5	**Task Name:** Lab-scale flow cell **Task Description:** Build and evaluate a lab-scale electrochemical purification flow cell to remove corrosive impurities from a flow of ternary MgCl2-KCl-NaCl molten salt.
6	**Task Name:** Purification byproduct mitigation **Task Description:** Mitigate risks associated with MgO buildup by developing protocols for removal of MgO. Evaluate risks of formation of H2, including flammability and explosion hazards as well as possible hydrogen embrittlement.

Task #	Task Name and Description
7	**Task Name:** Galvanic Corrosion Mitigation **Task Description:** Protect alloys from galvanic corrosion by evaluating down selected materials, avoiding dissimilar junctions where possible and providing engineering solutions, such as use of Mg sacrificial anodes, where needed.
8	**Task Name:** Evaluation of MgOHCl formation rate for its optimized removal **Task Description:** Determine rate of impurity formation in molten salts and rate of thermal decomposition of impurities to HCl and optimize purification accordingly, providing a design for continuous protection throughout the CSP plant.
9	**Task Name:** Package of results into a Tech-transfer document **Task Description:** Provide a document summarizing envisioned installation and operational requirements of purification cell, facilitating day-to-day operation by qualified technicians without advanced technical knowledge.

3. Project Results and Discussion:

All project tasks and milestones were completed on time and on budget, as summarized in Table 3-1 and detailed below.

Table 3-1. *Project Milestone and completion dates.*

Phase #	Task #	Milestone #	Milestone Name/Description	Planned End Date	Actual End Date	Milestone Type
1	1	1	**Demonstrate electrochemical removal of corrosive impurities:** The content of the corrosive impurity MgOHCl should be reduced by the proposed electrochemical method to [MgOHCl] ≤ 0.1 wt.%. Other impurities, such as Fe-containing compounds, will be reduced to values that will not be harmful to Gen3 CSP operation	12/31/20	12/31/20	Annual
1	2	1	**Evaluate Galvanic Corrosion:** The corrosion rate in molten chlorides of the dissimilar alloy junctions shall not be problematic, determined by various analytical techniques. Corrosion rates should be less than 20 micrometer/year.	03/31/21	03/31/21	Quarterly
1	3	1	**Cathodic Passivation Mitigation:**	03/31/21	03/31/21	Quarterly

Phase #	Task #	Milestone #	Milestone Name/Description	Planned End Date	Actual End Date	Milestone Type
			Demonstrate that MgO build-up can be physically removed from the purification device electrode as might be envisioned in a Gen3 CSP facility and does not drastically reduce the current efficiency of the electrochemical chamber to ≤ 95 % after 10 purification cycles compared with 1st cycle.			
1	4	1	**Preliminary Engineering Design:** For a given molten chloride flowrate, provide conceptual/preliminary electrochemical cell design for impurity removal. It will include area of electrodes, cell volume, resident time, possible electrodes' location, design of cell-bottom, and possible ways to remove H2(g) generated.	03/31/21	03/31/21	Quarterly
1	4	2	**Engineering Design Process:** Develop and appropriate design process to select the most effective reactor type for the purification cell.	03/31/21	03/31/21	Quarterly
2	5	1	**Identify the physics-based scaling relations:** To build confidence in the scaling relations, present the functions—after identifying the physics-based scaling relations—that will be used to attempt to validate against.	12/31/2021	12/31/2021	Quarterly
2	5	2	**Lab-scale flow cell:** Using design learnings from Budget Period 1, build and demonstrate feasibility of electrochemical flow cell for corrosive impurities from a flowing molten chloride salt.	12/31/2022	12/31/2022	Annual
2	6	1	**MgO mitigation:** Evaluate formation of MgO under flowing conditions and validate mitigation strategies.	6/30/2022	6/30/2022	Quarterly
2	6	2	**Hydrogen evolution assessment:** Evaluate formation of H_2 to ensure continuous safe operation of purification cell, and to prevent damage to CSP plant components.	6/30/2022	6/30/2022	Quarterly
2	7	1	**Galvanic corrosion mitigation:** Evaluate galvanic couples for further down-selected Gen3 CSP material and advise on methods for avoiding galvanic corrosion damage.	12/31/2022	12/31/2022	Annual

Phase #	Task #	Milestone #	Milestone Name/Description	Planned End Date	Actual End Date	Milestone Type
2	8	1	**Evaluation of MgOHCl formation rate for optimized MgOHCl removal:** Optimize proposed purification flow cell design and performance based on anticipated rate of impurity formation, supported by kinetics of salt reaction with water and thermolysis of impurities.	12/31/2022	12/31/2022	Annual
2	9	1	**Packaging of results into a tech-transfer or "know-how" document:** Provide a document summarizing the envisioned installation and operational requirements of purification cell, facilitating day-to-day operation by qualified technicians without advanced technical knowledge.	12/31/2022	12/31/2022	Annual

3.1. Task 1: Electrochemical minimization of corrosive impurities at the low temperature point as might be envisioned in a Gen3 CSP facility.

3.1.1. Task 1 Summary

Using a bench-scale batch reactor, electrochemical mitigation of the corrosive impurity MgOHCl was demonstrated at 500 ºC, the proposed low temperature point of a Gen3 CSP facility.[4] For each experiment, pure salt was doped via addition of NaOH, which reacted to form MgOHCl. Using the electrochemical method, MgOHCl was then reduced to ≤ 0.1 wt.%, fulfilling **Milestone 1.1.1.** This is illustrated in Figure 3.1.1-1.

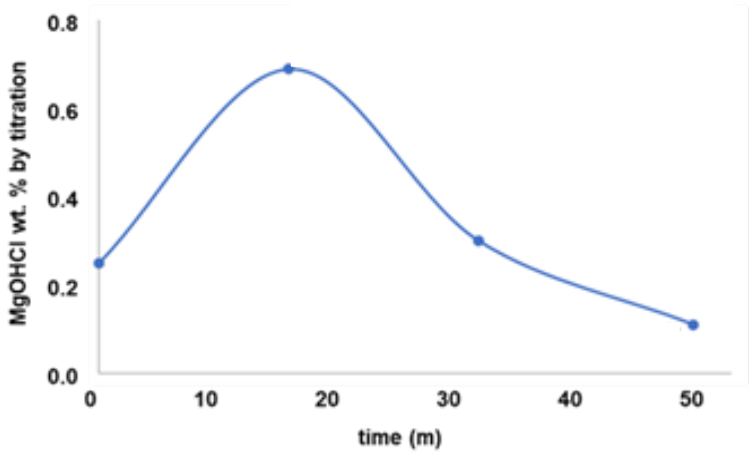

Figure 3.1.1-1. *MgOHCl wt. % over time during purification experiments in the bench-scale batch reactor. NaOH was added at t = 0m. Peak MgOH concentration was*

achieved at approximately 15 minutes. At this point, the electrochemical method was utilized to reduce the MgOHCl wt. % to ≤ 0.1 wt. %.

3.1.2. Identification of corrosion pathways

According to previous research, molten chloride salt doesn't intrinsically cause corrosion to metal alloys.[21, 22] This is illustrated in Figure 3.1.2-1, an Ellingham diagram, which was constructed for various alloying constituents using the thermodynamic software HSC v8.

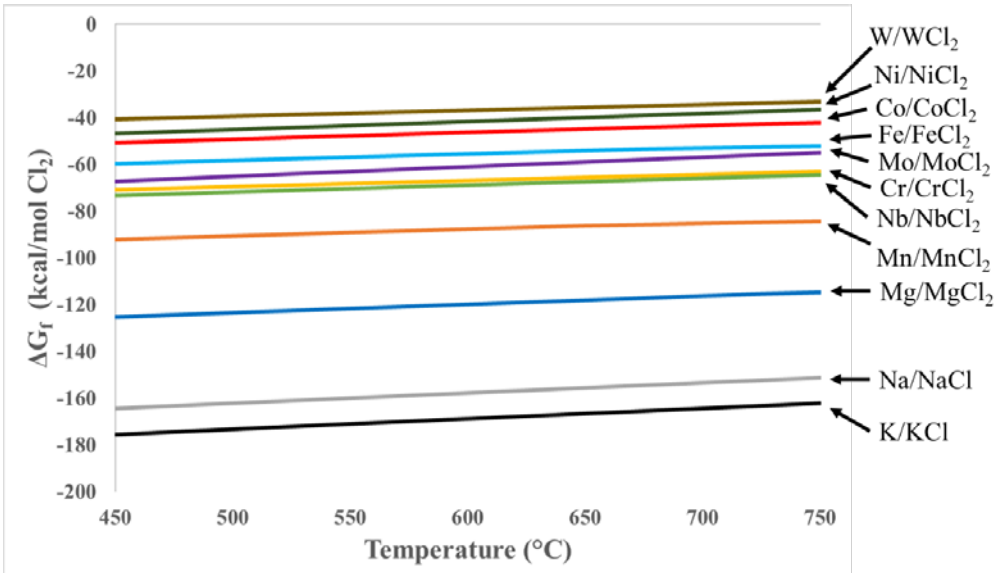

Figure 3.1.2-1. *Gibbs-Free energy of metal-metal chloride as a function of temperature.*

The most stable chlorides (most negative ΔG_f) are K, Na, and Mg. Therefore, common alloying constituents (e.g., Fe, Cr, Ni) should theoretically remain stable in the chloride salt.

However, corrosion occurs due to the presence of oxide and hydroxide impurities in the Mg-K-Na chloride salt. These impurities arise due to the hygroscopic nature of $MgCl_2$, which leads to the following reactions:

$$MgCl_2 + H_2O \rightleftharpoons MgOHCl + HCl \qquad [3.1\text{-}1]$$

$$MgOHCl \rightleftharpoons MgO + HCl \qquad [3.1\text{-}2]$$

$$O_2 + 4Cl^- \rightleftharpoons 2O^{2-} + 2Cl_2 \qquad [3.1\text{-}3]$$

The hydrochloric acid, hydroxide, and oxide species in the salt then follow degradation reactions with alloying constituents M (e.g., Cr, Fe, Ni):

$$xHCl + M \rightarrow MCl_x + \frac{x}{2}H_2 \qquad [3.1\text{-}4]$$

$$xMgOHCl + M \rightarrow xMgO + MCl_x + \frac{x}{2}H_2 \quad [3.1\text{-}5]$$

$$\frac{x}{2}O_2 + yM \rightarrow M_yO_x \quad [3.1\text{-}6]$$

Thus, the main cause of corrosion is MgOHCl, which reacts with alloying constituents via reaction in the order listed in Figure 3.1.2-1. This is consistent with previous work by Zhao et al[23]. which showed a strong correlation between the concentration of MgOHCl and corrosion rates of Ni-alloy. Further studies indicated that corrosion rates of Ni-alloys and even stainless steels can be kept to ~25 μm/year if the concentration of MgOHCl is kept to ≤ 1,000 ppm.

Besides MgOHCl, oxygen plays a minor role in corrosion.[22] Typically, the formation of oxides creates a protective oxide layer and prevents further corrosion, e.g., stainless steel forms a passivating chromium oxide layer. However, most oxides are not stable in the presence of chloride as is shown in a chloride-oxide stability diagram, Figure 3.1.2-2. The metal chloride-oxide species can be categorized into three systems:

- Above the parity line (ΔG_f oxide = ΔG_f chloride) the chlorides species are thermodynamically more favored (K, Na, Mn).
- Below the parity line, the oxide species are more favored (Al, Nb, Mo, W).
- Along the parity line, both chloride and oxide species are in equilibrium with each other (Mg, Cr, Fe, Co, Ni).

The K and Na chlorides are highly resistant to oxidation and can be considered stable in the presence of oxygen and moisture, whereas Mg is not. Additionally, upon oxidation of Mn, Cr, Fe, Co, and Ni, the oxide will react with chloride ions to form a more stable chloride. This is known as the chlorination-oxidation cycle and is the cause of high corrosion rates in stainless steel alloys, which have high Fe, Cr, and Mn content. The chloride-oxide stability diagram predicts that the preferential order of corrosion is Mn > Cr > Fe > Ni, which matches experimental observations. Furthermore, the corrosion of Ni-based alloys experience lower rates of corrosion due to the thermodynamic stability of Ni. Lastly, the corrosion resistance of Ni-alloys is enhanced due to the inclusion of W, Mo, and Nb, which forms a stable oxide that can serve as a passivating layer.

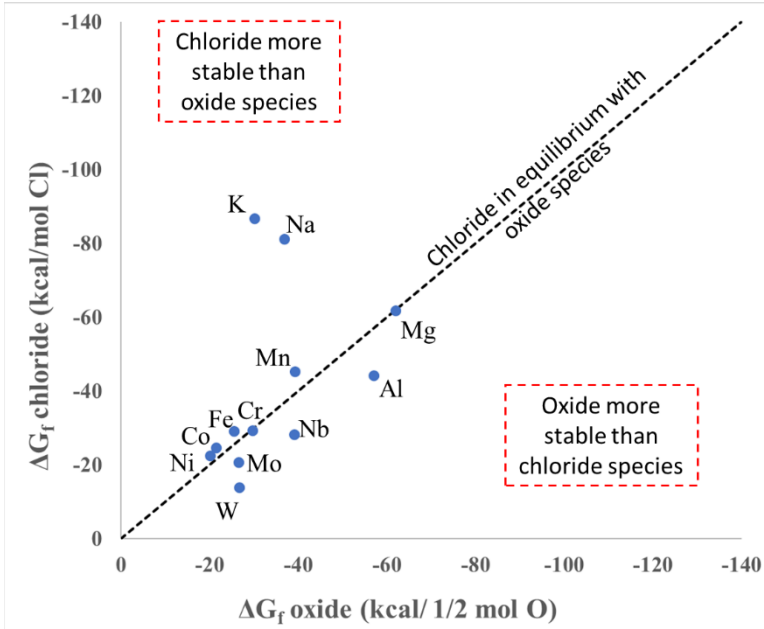

***Figure 3.1.2.-**2 Chloride-oxide stability diagram of various alloying constituents at 500 °C.*

3.1.3. Simulating Gen3 CSP molten salt conditions

Reagent grade MgOHCl is not readily available and is difficult to synthesize in high purity. In literature, corrosion studies typically use NaOH to dope the chloride salt with MgOHCl according to reaction[7, 15, 24-30]:

$$NaOH + MgCl_2 \rightarrow MgOHCl + NaCl \qquad [3.1.3\text{-}1]$$

HSC was utilized to confirm reaction. Figure 3.1.3-1 shows addition of NaOH to the system has the same effect as moisture and validates the use of NaOH dope salt with MgOHCl for purification experiments.

Thus, to introduce MgOHCl impurity into the molten chloride salt mixture, NaOH pellets (~1.0 g, ≥97.0%, Macron) were directly added to the molten chloride salt mixture via an open reactor port according. To ensure an accurate mass of NaOH, the pellets were dried overnight at 120 °C and stored in the glovebox until use. After NaOH introduction to the salt, MgOHCl formed rapidly, producing MgOH+ that was observed by CV.

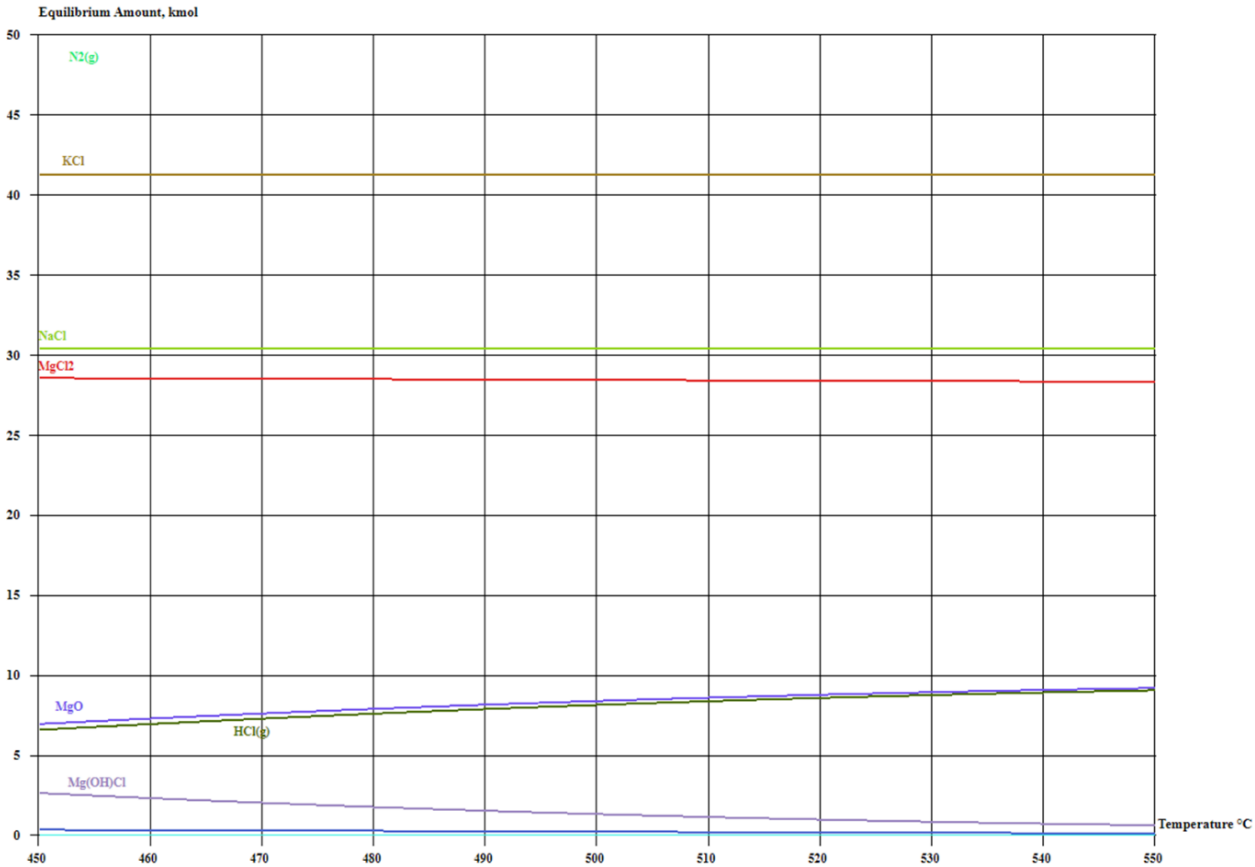

Figure 3.1.3-1. *Mg-K-Na chloride salt blend with nitrogen and NaOH.*

3.1.4. Bench-Scale Electrochemical Batch Reactor

A ternary blend of chloride salts (MgCl+ (45.98 wt.%), KCl (38.91 wt.%), NaCl (15.11 wt.%) was prepared in batches of 550 g. MgCl2 (99% Anhydrous, Alfa Aesar), KCl (≥ 99%, Avantor), and NaCl (≥ 99%, Fisher-Chemical) were used as received. The ternary blend was prepared and stored in an argon glovebox to avoid hydrolysis of MgCl2 (≤0.5 ppm H_2O, ≤0.1 ppm O_2, Inert Technologies).

Salt was melted using the procedure adapted from Ding et al.[15] Prior to melting, the salt was put under vacuum (0.85 bar) for 30 minutes in a nitrogen-filled glovebox. The salt was then transferred to the reactor vessel and heated at a rate of 5 ℃/min to 200 ℃ and held at temperature for 90 minutes. Afterwards, the salt was heated to the temperature of the experiments (475, 500, or 525 ℃) at a rate of 5 ℃/min. Throughout the heating procedure and experiments, ultra-high purity nitrogen (99.999%, ≤1 ppm H2O, ≤1 ppm O2) was flowed through the reactor at 100 mL/min to avoid moisture and oxygen ingress.

Figure 4.1.4-1 shows the experimental benchtop batch reactor used for all experiments related to the electrochemical behavior of MgOHCl reduction.

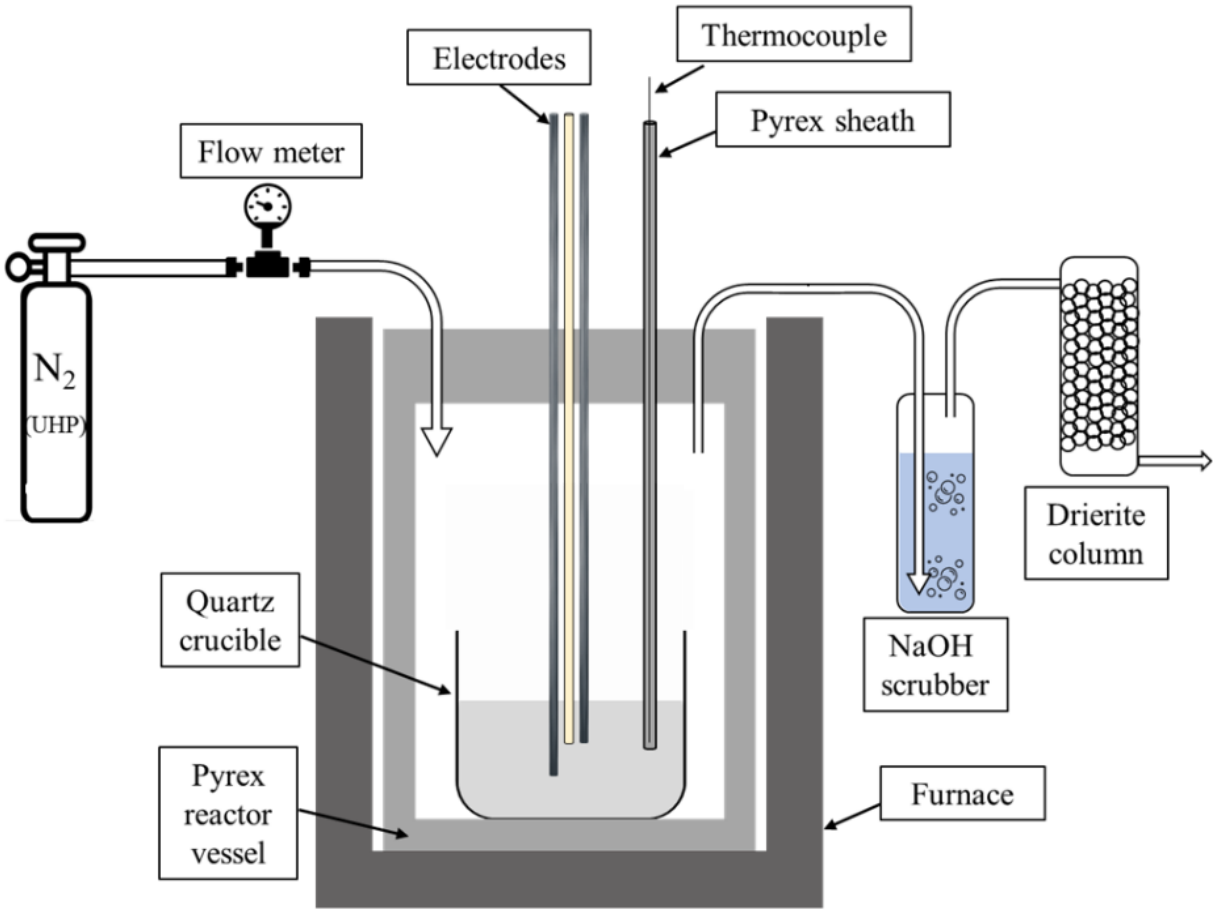

Figure 4.1.4-1. *Schematic of bench-scale batch electrochemical purification reactor.*

All experiments were conducted in a custom 8-port Pyrex reactor lid and vessel from Allen Scientific Glass Inc. The Pyrex reactor allowed visual observation of the salt and gas evolution during experiments. Within the Pyrex reactor, a fused quartz crucible (Advalue Technology) was used to hold the chloride salt mixture to avoid damage to the reactor vessel from the salt during cooling. A Pyrex thermocouple sheath with a k-type thermocouple (Omega Engineering) was directly inserted into the molten chloride salt to monitor the temperature set by a programmable furnace (Mellen). As noted, ultra-high purity nitrogen (99.999%, ≤1 ppm H2O, ≤1 ppm O_2) flowed at 100 mL/min to avoid moisture and oxygen ingress into the reactor. The cover gas outlet passed through a 1.0 M NaOH scrubber and a desiccator column (Drierite) before exhausted. The NaOH scrubber was used to remove any potential HCl gas, and a desiccator was used to remove any moisture before venting the off gas into the exhaust line.

A three-electrode setup was used for the electrochemical experiments. An Ag/AgCl reference electrode was fabricated as described by Choi et al. and Wang et al. [57,64]. A 0.5 mm diameter Ag wire (99.9%, AlfaAesar) was inserted into a 6.35mm diameter alumina sheath (Advalue Technology). The bottom ~3 cm of the alumina sheath was polished down to ~15 μm wall thickness. Inside the alumina sheath 2.5 g of chloride salt mixture was added with 1 wt.% of AgCl (99.9%, ThermoScientific). Table 3.1.4-1 summarizes the electrode material and purpose for each experiment.

Table 3.1.4-1. *Electrode Material and purpose for each experiment.*

Method	Application	Electrode Material		
		Working	Counter	Reference
Cyclic voltammetry (CV)	Determine reduction potential of MgOH+, diffusion coefficient of MgOH+, charge transfer coefficient, and standard rate constant	W	W	Ag/AgCl
Controlled potential coulometry (CPC)	Determine mechanism of current behavior on cathode	W	Mg	Ag/AgCl
Chronopotentiometry (CP)	Determine diffusion coefficient of MgOH+	W	W	Ag/AgCl
Square wave voltammetry (SWV)	Determine number of electrons transferred and charge transfer coefficient	W	W	Ag/AgCl

The W working electrodes were 1.49 mm in diameter. The W counter electrodes were 4.76 mm in diameter to ensure the working electrode was not surface area limited by the counter electrode. Similarly, the Mg counter electrode in CPC experiments was 7.85 mm in diameter. The W and Mg electrodes were purchased from Midwest Tungsten Service (99.95%) and Goodfellow (99.9%) respectively. Before each experiment, the electrodes were polished to a mirror-like finish using 800, 1200, and 2000 grit sandpaper. After polishing, the electrodes were stirred in 2% nitric acid solution for 1 minute and then rinsed with de-ionized water. Once dry, the electrodes were immersed in the salt for at least one hour to ensure thermal equilibrium and a stable open-circuit potential (<0.5 mV/s drift).

All electrochemical experiments were conducted using a Gamry 1010 workstation. The potentiostat used in this study was not capable of positive feedback iR compensation. Therefore, the uncompensated resistance was measured via electrochemical impedance spectroscopy and found to be 0.1696 Ω. iR compensation was done post experiment in Gamry's post processing software.

The surface area of the electrode was calculated by physically measuring the immersion height via calipers after the experiment. This method has been demonstrated to be accurate within 0.5 mm immersion depth for molten salts.[14] The working electrode was typically immersed 2-3 cm, resulting in a calculated surface area error of less than 2%. Visual observation of the experiments confirmed no salt wicking up the electrodes.

An electrochemical cleaning step was necessary to obtain reproducible data, likely due to the formation of the insoluble product MgO on the working electrode. An electrochemical cleaning consisted of application of an anodic stripping potential of +0.8

v vs. W for 3 seconds, followed by holding at the open circuit potential (OCP) for 240 seconds.

3.1.5. Identification and reduction of impurities to ≤ 0.1 wt.% using electrochemical method

The concentration of MgOH+ was calculated using cyclic voltammetry.[16] The concentration of MgOH+ is directly related to the current density of the MgOH+ reduction peak (Figure 3.1.5-1) multiplied by a constant $c_{CV}(T, v)$ (Equation 4.1.1-1).

$$C_{MgOH^+} = i_{MgOH^+} \cdot c_{CV}(T, v) \qquad [3.1.5\text{-}1]$$

Where $c_{CV}(T, v)$ is a constant as a function of temperature and scan rate (ppm O/(mA/cm2)), i_{MgOH^+} is the current density of the MgOH+ reduction peak (mA/cm2), and C_{MgOH^+} is the concentration of MgOH+ in the salt (ppm), which was determined via acid-base titration.

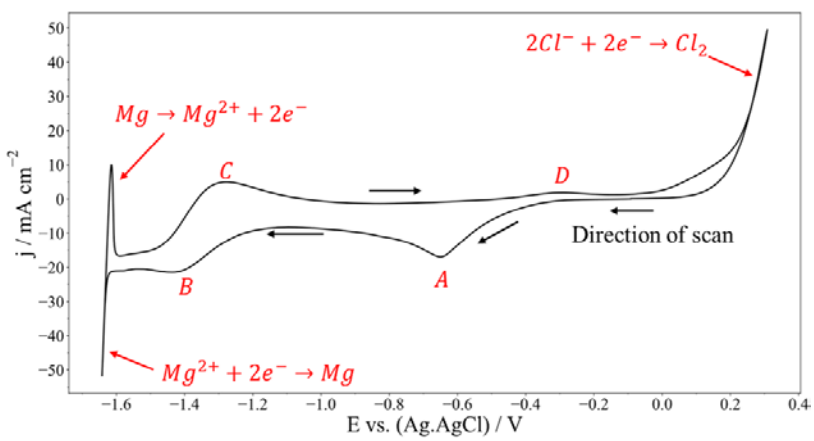

Figure 3.1.5.-1 *Cyclic Voltammagram obtained on W working electrode in chloride salts at 500 ºC and 250 mV/s.*

To determine $c_{CV}(T, v)$, salt aliquots were taken immediately after a CV scan. The salt aliquots were drawn using a Pyrex tube attached to a handheld vacuum pump. The salt was stored under vacuum and then prepared for titration inside an argon glovebox.
To prepare the salt for titration, ~0.5 g of salt was dissolved in 0.1 M nitric acid via stirring for 1 hour at 500 rpm. The acid was then titrated with 0.05 M NaOH solution to calculate the total acid consumed. It was assumed all acid consumed was due to MgOH+ given the low solubility of MgO.
The titrations for each aliquot were done in triplicates to report an average and standard deviation. The $c_{CV}(T, v)$ were determined and summarized in Table 3.1.5-1.

Table 3.1.5-1. *Experimentally determined concentration constant for CV at a scan rate of 250 mV/s at various temperatures.*

Temperature	$c_{CV}(T, v)$
(°C)	(ppm O)/(mA/cm^2)
475	43.22 ± 5.65
500	41.79 ± 2.91
525	37.73 ± 3.86

From this table, the values for $c_{CV}(T, v)$ decrease with increasing temperature as expected. Furthermore, $c_{CV}(T, v)$ at 500 °C agrees well with the value of 38.2 ± 7.2 (ppm O)/(mA/cm^2)obtained in literature.

3.2. Task 2: Galvanic corrosion control at the low and high temperature points as might be envisioned in a Gen3 CSP facility.

3.2.1. Task 2 Summary

Galvanic corrosion was identified when using H230 or 342H in combination with C276. Compared to C276, H230 and 342H are less noble. Therefore, when in electrical contact with C276 in the presence of an electrolyte (the molten salt), depletion of alloying in elements in H230 and/or 342H occurs. This was demonstrated by mass loss experiments and by SEM, illustrated in **Figure 3.2.1-1.** Cathodic protection using an Mg sacrificial anode was proposed as a potential solution for this problem. This work fulfilled **Milestone 1.2.**

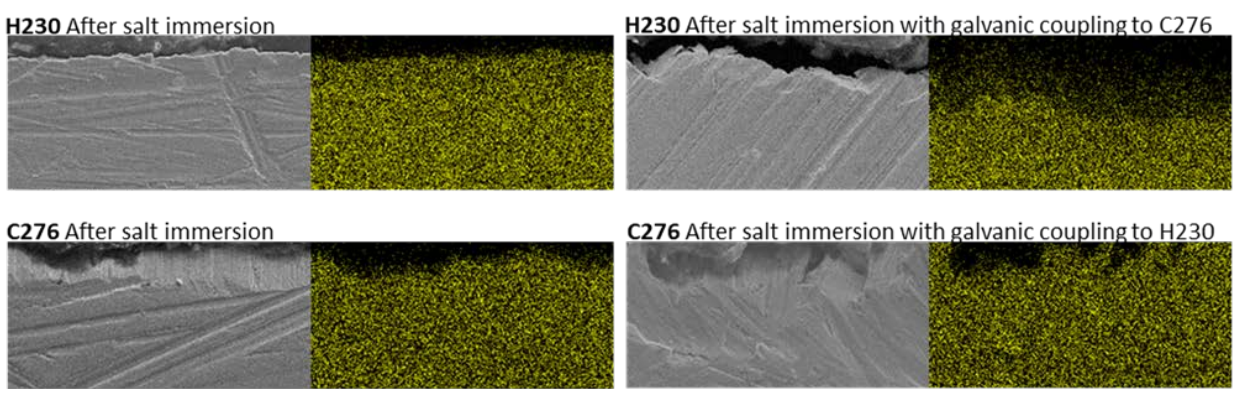

Figure 3.2.1-1. *Elemental mapping of Cr (SEM-XPS) in alloy cross sections after immersion in molten chloride salt at 450 ºC for 72 hours. For galvanically coupled samples, Cr depletion is observed in H230.*

3.2.2. Preliminary galvanic corrosion evaluation in Phase 1

We designed an experimental setup to evaluate whether Mg metal can be used for cathodic protection, preventing galvanic corrosion. This experimental setup is shown in Figure 3.2.2-1. Furthermore, factors like reduction potentials of different materials could be assessed.

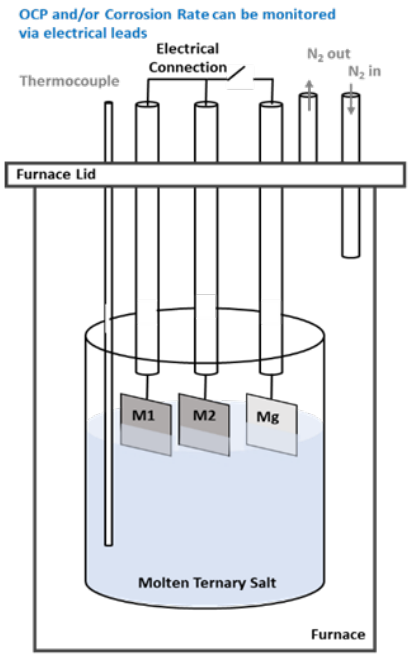

Figure 3.2.2-2. *Schematic of setup for evaluation of galvanic corrosion.*

Two primary challenges were addressed in designing this setup. First, a method for attaching the metals to electrical leads, to ensure galvanic contact, was needed. Welds, which we used for initial assessments, were determined to be not preferred, as the welds could alter metal surface characteristics. Investigation of weldments, while important, is beyond the scope of this project (they are being investigated by other Salt Collective members).[4] Therefore, various methods of attaching electrical leads to alloy samples and Mg metal were investigated, including tap and dye threading, use of alligator clips, and Ni wire threaded through a predrilled hole. We concluded that tap and dye threading runs the risk of the sample falling off into the salt with minimal corrosion and or sample dissolution. The use of an alligator clip, while effective at maintaining a secure clamp even during corrosion, was not feasible due to the possible instability of alligator clip materials at high temperatures. Ultimately, drilling a hole in each sample and threading a wire lead through was determined to be the most robust method.

Immersion depth of samples was also evaluated. In cases where samples were immersed entirely, it was important that wire leads did not make electrical contact with the salt. In this case, wire leads could participate in galvanic corrosion. Therefore, the use of boron nitride coating was investigated to coat wire leads and prevent electrical contact with salt. While this method works initially, it is susceptible to failure upon corrosion/dissolution of samples, when fresh wire surfaces could be exposed. Thus, a decision to immerse samples only partly in salt was made. This method was validated by several experiments showing that salt height does not change substantially during experiments, and thus consistent surface area exposure can be maintained.

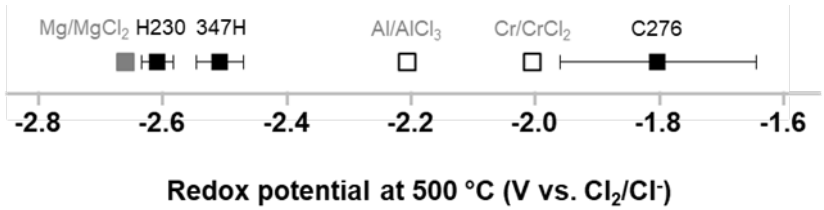

Figure 3.2.2-2. *Experimental values of potential of containment alloys under consideration. Also shown are literature potential of $Mg/MgCl_2$, $Al/AlCl_3$, and $Cr/CrCl_2$, because these elements are commonly used in alloys and subject to depletion.*

These results suggest that galvanic corrosion is a concern and confirm that Mg is less noble than any alloys under consideration. Therefore, Mg is an acceptable material for a sacrificial anode. Thus, this work meets the milestone. However, in this data, both H230 and 347H appeared less noble than expected. In fact, the redox potentials of these materials were very close to Mg. While the principle of cathodic protection using Mg would still work in this case, possible reasons for the unexpected reaction potentials were cause for further evaluation.

First, we considered the composition of these two materials. Both materials contain Cr, which is less noble than many materials and therefore a common corrosion concern. In addition, H230 also contains Al, which has an even more negative redox potential than Cr in molten salts.[1, 8, 15, 19-22, 31-33] However, in our setup, H230 and 347H appeared to have even more negative potentials than these components. Two possible explanations are proposed. 1) In the alloy, it is possible that due to interatomic interactions, components are more easily removed than in the pure metals. In this case, the alloys could be less noble than their component elements. 2) In our setup, Mg is immersed in the salt with the alloy samples. While the salt temperature is well below the melting point of Mg, some sources indicate that Mg dissolution is nonzero. Thus, it is possible that Mg from the molten salt deposited on the surface of alloy samples, altering electrochemical behavior. Therefore, although the results presented here meet the milestone since corrosion of these metals was not observed with Mg, continued work was suggested for Phase 2.

3.2.3. Mass loss tests for galvanic corrosion

Mass loss tests were also performed on H230 samples coupled to C276, and on 347H samples coupled to C276. All immersion and mass loss tests were conducted according to corrosion evaluation protocols developed by The Salt Collective[19], and standard deviations were obtained by obtaining cathodic protection data for at least three samples in each case. Dr. Youyang Zhao advised us on the procedure. Samples were immersed in salt at 450-500ºC for up to 100. Two types of testing were performed:

1. Unprotected galvanic couples: Samples of dissimilar alloys were immersed in molten chloride salts such that they each had 4 cm^2 of surface area in contact with the salt. Electrical contact was achieved with Ni wire, attached to the part of the samples that protruded above the salt level, such that the Ni wire was not in contact with the salt.
2. Galvanic couples protected with Mg metal: For evaluation of Mg-based cathodic protection, the method used for galvanic control sample 2 was employed, but with the addition of an Mg coupon, which was also placed in the molten salt and in electrical contact with the alloy samples.

Consistent with results based on electrochemical evaluation, H230 and unprotected 347H lost mass when coupled to C276. When this sample was sonicated in water to remove surface salt, the water turned black, consistent literature reports of Cr species washed off of samples which had undergone galvanic corrosion. After 100 h at 500ºC, these samples lost *ca.* 4 mg. Using the surface area exposed and density of H230, this translates to a corrosion rate of 90 µm per year, outside the Salt Collective threshold of 20 µm per year. Similar calculations performed for 347H samples that were in contact with H230 showed a corrosion rate of 220 µm, almost ten times the acceptable level. This is clear evidence that in cases of galvanic coupling to H230, cathodic protection will be required. All other alloy samples gained mass, consistent with deposition of Mg on alloy surfaces.

Galvanic corrosion analysis was consistent with SEM imaging and XPS analysis from Q2. The results of this analysis are shown in Figure 3.2.1-1. While no pitting or cracking can be observed in any sample, elemental mapping of Cr shows a *depletion of Cr near the surface of H230* with galvanic coupling. Irregularities in the surface make precise evaluation of the thickness of this depletion zone difficult, but it is at least on the order of tens of micrometers. This indicates that galvanic corrosion may be a problem, and that a solution for galvanic corrosion is necessary.

3.3. Task 3: Effective removal and collection of cathodic MgO build-up.

3.3.1. Task 3 Summary

The possibility of cathodic passivation due to MgO buildup on the surface of the cathode was identified as a risk of the electrochemical approach. MgO is a byproduct of purification, according to reaction [1-5]. Since MgO is an insulator rather than a conductor, if MgO adhered to the electrode surface, over time, it would passivate the electrode and stop the electrochemical process. However, after 10 purification cycles in the batch reactor, current efficiency was less than 10% lower compared to initial current efficiency (**Figure 3.3.1-1**), showing that cathodic passivation is not a significant risk and fulfilling **Milestone 1.3.**

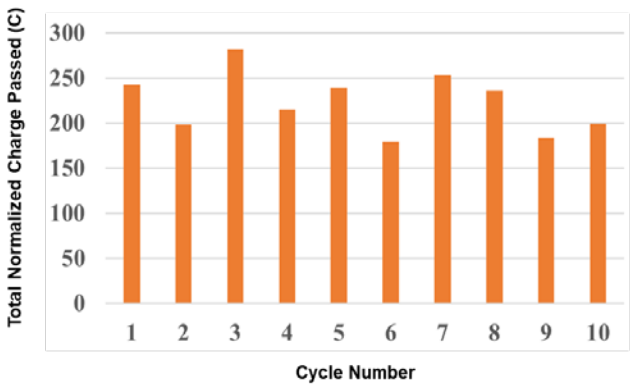

Figure 3.3.1-1. *Normalized charge passed for each of ten 30-minute purification cycles performed consecutively with the same electrode, without cleaning steps. While values vary between cycles, there is no overall trend of passivation. For example, the total charge passed in cycle 10 is equal to the total charge passed in cycle 2 and less than 10% decreased compared to cycle 1.*

3.3.2. MgO Analytical Methods

It was first necessary to evaluate the form factor of MgO produced by the electrochemical purification cell. There were two possible form factors considered:
1) The MgO could form an oxide layer on the surface of the W electrode. Evidence for this occurrence was observed in the literature.[15]
2) The MgO could form particulates in the bulk salt, which would eventually settle to the bottom of the crucible.
Based on our analysis, both form factors occur, but form factor 1) flakes off over short timescales and does not build up. Thus, form factor 2) is dominant.

Analysis of samples scraped from electrodes by XRD was conducted, confirming the presence of MgO. Salt hydrates were also present. However, these are likely due to the exposure of the sample to air during the measurement.

To determine the size of MgO within the salt, upon completion of an electrolysis experiment, the ternary chloride salt was cooled to room temperature under a flow of argon gas. Once cooled, the crucible containing the salt was transferred to a 2-L beaker and filled with deionized water. The beaker with the salt crucible was left on a stir plate for 48 h at 250 rpm to dissolve the salt. The contents of the beaker were then filtered using 22-µm pore size filter paper and the filtrate was weighed after air drying for 24 h. Only 4.7 mg of solid material was recovered. This is far lower than the amount of MgO expected based on MgOHCl removed. However, the filtrate was observed to have a milky-greyish appearance. Therefore, it is likely that MgO particulates smaller than the filter pore size of 22 µm were still suspended in solution, indicating that MgO particulate size is very small under laboratory conditions.

Further evidence that little MgO particulate matter was present in the salt was found by titration. For many of the samples, even when MgOHCl wt. % was reduced, indicating that MgO had formed, MgO wt. % in the salt was very low, or in some cases, not detectable. This could be partly due to settling of MgO on the bottom of the crucible, which would give low titration results for MgO samples taken from the middle of the crucible. There is some evidence that this occurs, as titration taken from the bottom of the crucible does, in some cases, have higher MgO content after many rounds of electrolysis. However, according to particulate settling data collected by Dr. Youyang Zhao, settling of salt particles from the top to the bottom of the crucible would take more than 1 h for particle sizes less than 22 µm. Since titration samples were withdrawn during an immediately following electrolysis, it is not reasonable that all the particles could have settled in this timeframe.

Since we have shown that MgO can temporarily deposit on the cathode in our system, it is important to show that the cathodic effect, passivation of the electrode due to an insulating buildup, will not be problematic. Our results show that it does not appear that this buildup is a significant hurdle. There is an initial sharp decrease in the current density, followed by a roughly linear decrease observed from ca. t=3 min to the end of the experiment.

We attribute the initial sharp decrease not to cathodic passivation, but rather, to mass transport limitations. Initially, the concentration of the impure species is high at the electrode surface. However, a depletion layer quickly begins to build around the electrode, at which point current density is limited by the slow diffusion of the impure species to the electrode surface.

The steady decrease observed after 3 min occurs at a rate of ca. 0.03 % per minute. Since most of the purification takes place within 30 min of electrolysis as shown by kinetics evaluation above, we calculate that the *maximum current decrease attributed to the cathodic effect during one purification cycle is ca. 0.96%.* However, we also note that this drop can be partly attributed to purification, i.e., reduction of the wt. % impurity of the reacting species in the molten salt. The fact that titration shows the decreasing current is occurring simultaneously with decreasing $MgOH^+$ clearly indicates that removal of this species is a contributing factor.

To further confirm that current efficiency does not drop after multiple cycles and to meet our milestone, we performed a series of 10 electrolysis cycles. Results are illustrated in Figure 3.3.1-1. After each cycle, NaOH was added to the purification cell without removing the electrodes. We calculated the total charge passed during each cycle. The total charge passed varies significantly from cycle to cycle, possibly due to mass transport variations in our unstirred batch reactor. However, there is no overall decreasing trend, indicating that current efficiency is not progressively dropping over time.

Thus, we have demonstrated that in the laboratory setup, current efficiency loss attributed to cathodic passivation is not occurring to a problematic extent. This result, taken with the above calculation that cathodic passivation is responsible for at most as loss of ca 0.96% per purification cycle compared to initial current efficiency, fulfils the target of demonstrating ≤ 10 % current loss due to cathodic passivation over the as a function of time compared to initial current efficiency.

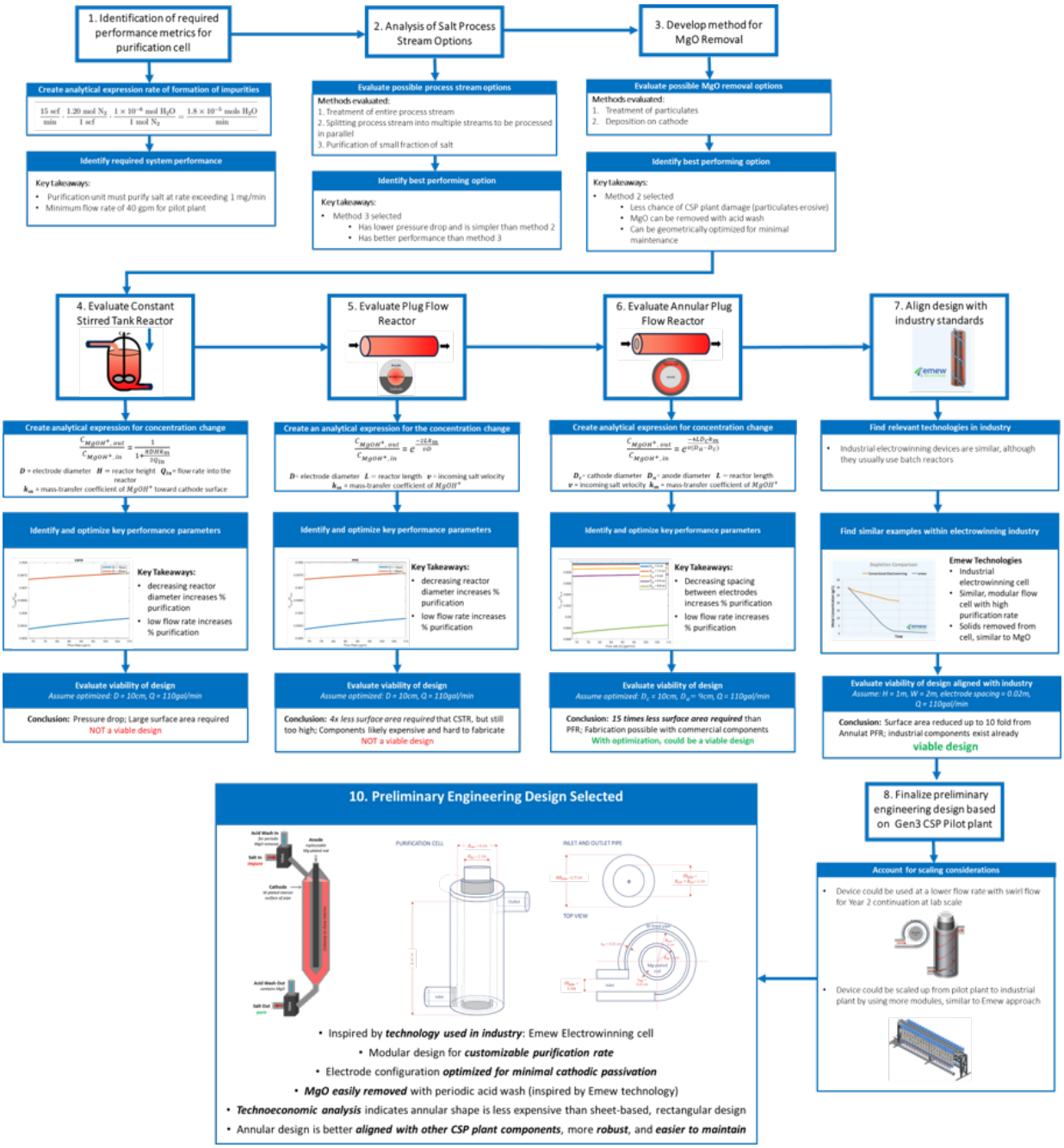

Figure 3.4.1-1. *Flow chart illustrating the design process for the electrochemical purification cell.*

3.4. Task 4: Conceptual/preliminary engineering design of an electrochemical cell for purification of molten chlorides for the low temperature point as might be envisioned in a Gen3 CSP facility.

3.4.1. Task 4 Summary

A preliminary engineering design for an electrochemical purification cell was designed using the process depicted in **Figure 3.4.1-1.** Performance metrics were identified,

options for integration of purification with a flow of molten salt in a Gen3 CSP plant were considered, common reactor types were evaluated, and ultimately, a preliminary design for an annular continuous flow-reactor was selected. Production of the preliminary engineering design fulfilled **Milestone 1.4.1.**, while creation of the systematic approach detailed in the flow chart fulfilled **Milestone 1.4.2**.

3.4.2. Reactor Type Down Selection

The design and optimization of a reactor revolves around understanding transport processes with chemical change. In this work, the transport process is the flow of molten chloride salt including the corrosive impurity MgOHCl ($MgOH^+$ in ionic form). The electrochemical change is the reduction of $MgOH^+$ on an electrode surface. It is assumed that the molten chloride salt starts as purified. Therefore, the electrochemical purification process needs to remove impurities immediately after formation. Given the low concentrations of MgOHCl impurity (≤ 1 wt.%), the performance of an electrochemical purification cell is related to the mass-transfer rate of $MgOH^+$ in the molten salt towards the cathode surface for electrochemical reaction.

As a starting point, idealized reactor designs were investigated due to the ability to derive analytical equations. The three designs considered were: 1) continuous stirred-tank reactor (CSTR), 2) plug flow reactor (PFR), and 3) annular shaped PFR. The three reactor types and designs are shown in Figure 3.4.2-1.

The reactor designs are geared toward volume-based reactions, whereas in this work, the focus is on surface based reactions. However, it is still possible to extract value information on design parameters versus reactor performance. The analytical solutions of the CSTR, PFR, and annular PFR are summarized in Table 3.2.2-1.

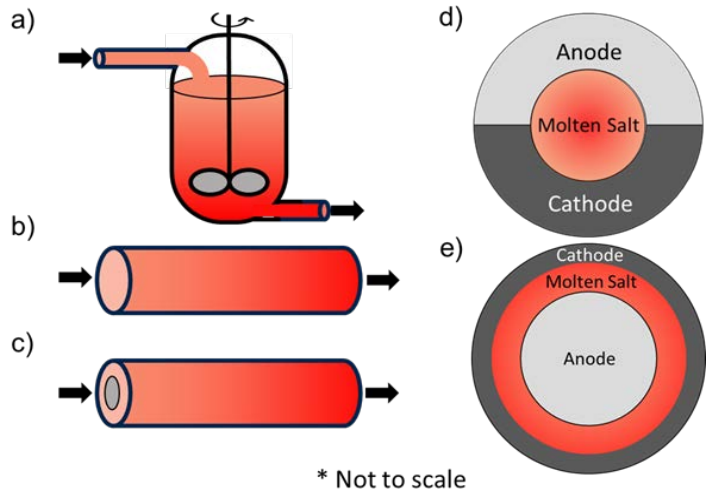

Figure 3.4.2-1. *Conceptual designs of electrochemical purification cells. a) CSTR, b) PFR, c) annular PFR, d) cross section of CSTR and PFR, e) cross section of annular PFR.*

Table 3.4.2-1. *Concentration profiles derived from conservation of mass for various reactor types.*

Concentration Profile	CSTR	PFR	Annular PFR
$\frac{c_{MgOH^+,out}}{c_{MgOH^+,in}} =$	$\frac{1}{1+\frac{\pi D H k_m}{2Q_{in}}}$	$exp\ (\frac{-2Lk_m}{Dv})$	$exp\ (\frac{-4D_{outer}Lk_m}{(D_{outer}^2 - D_{inner}^2)v})$

Where, $c_{MgOH^+,in}$ and $c_{MgOH^+,out}$ are the concentration of $MgOH^+$ going in and out of the reactor, respectively; *D* is the diameter of the molten-salt flow area, *H* is the height of the CSTR, *L* is the length of the PFRs, Q_{in} is the volumetric flow rate of the molten salt going into the reactor, k_m is the mass-transfer coefficient of $MgOH^+$ toward the cathode surface, *v* is the velocity of the molten salt going into the reactor, and D_{outer} and D_{inner} are the outer and inner diameter of the annular PFR, respectively.

The mass-transfer coefficient, k_m, can be estimated using the Sherwood number, Sh.

$$Sh = \frac{k_m}{\mathcal{D}_{MgOH^+}/L} \qquad [3.4.2\text{-}1]$$

Where $\mathcal{D}_{MgOH^+}$ is the diffusion coefficient of $MgOH^+$ (m^2/s), and L is the characteristic length (m). From cyclic voltammetry experiments, we calculated $\mathcal{D}_{MgOH^+}$ to be 7.334e-6 cm^2/s at 500ºC.

The Sherwood number, Sh, can be estimated using the Chilton-Colburn j-factor analogy for mass transfer, which has been shown to fit data well for diffusion-limited electrode processes with high Schmidt values (693–37,200) .

$$j_M = \frac{Sh}{ReSc^{1/3}\sqrt{\frac{f}{2}}} = 0.0575 + 0.1184Sc^{-\frac{1}{3}} \qquad [3.4.2\text{-}2]$$

Where j_M is the j-factor analogy for mass transfer, *Re* is the Reynolds number, *Sc* is the Schmidt number, and f is the Fanning-friction factor.

The Reynolds number is calculated based on the fluid properties and the equivalent diameter of the reactor.

$$Re = \frac{\rho u D_e}{\mu} \qquad [3.4.2\text{-}3]$$

Where ρ is the density (kg/m^3), u is the velocity (m/s), D_e is the equivalent diameter (m), and μ is the viscosity (Pa·s).

The Schmidt number is calculated based on the fluid and $MgOH^+$ properties.

$$Sc = \frac{\mu}{\rho D_{MgOH^+}} \qquad [3.4.2\text{-}4]$$

In our system *Sc* is 2726 at 500ºC. This is considered a high Sc system.
The equivalent diameter, D_e, is defined as

$$D_e = 4r_H \qquad [3.4.2\text{-}5]$$

Where r_H is the hydraulic radius defined as

$$r_H = \frac{A}{S} \qquad [3.4.2\text{-}6]$$

Where A is the cross-sectional area of the flow, S is the wetted perimeter of the cross section.
Furthermore, the mean residence time of the reactor is important to estimate the salt throughput.

$$\tau = \frac{V}{Q} \qquad [3.4.2\text{-}7]$$

Where τ is the mean residence time (s), V is the volume of the reactor (m^3), and Q is the salt flow rate (m^3/s).

The performance of the CSTR and PFR was assessed as a function of flow rate and pipe diameter $D_{electrode}$ (equal to D_{inner}) at a fixed height of CSTR and length of PFR of 10 m. A starting impurity concentration of 1 wt.% was assumed. The results are shown in Figure 3.4.2-2.

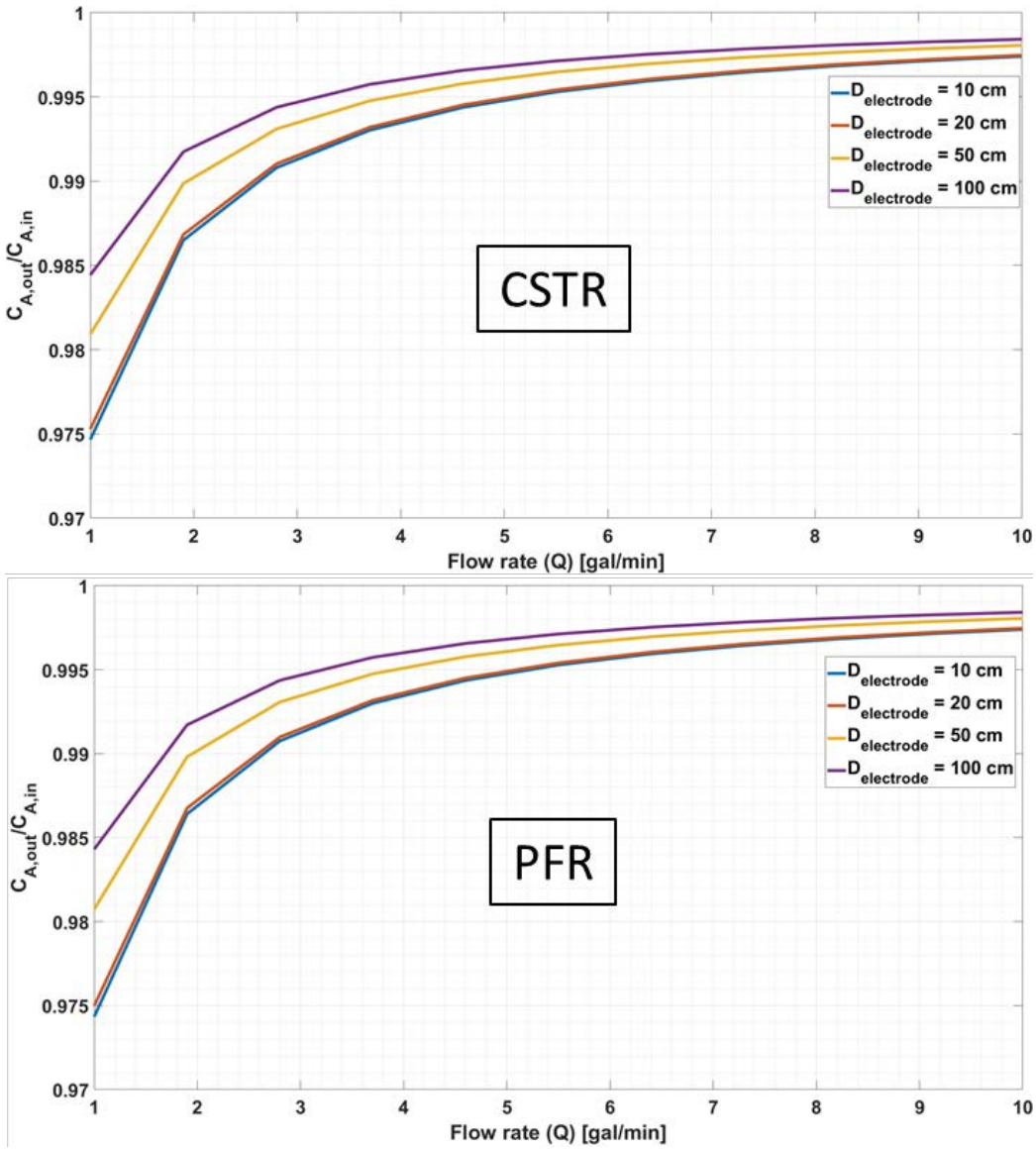

Figure 3.4.2-2. *Reactor performance versus pipe diameter and flow rate.*

Higher flow rates result in lower residence time in the reactor and therefore reduce reactor performance. Also, smaller pipe diameters result in better reactor performance. This is likely because of the greater ratio of electrode area to reactor volume. Furthermore, under these conditions, the CSTR and PFR perform identically. However, both reactors perform poorly at high flow rates—even at a flow rate of 1 gal/min and a pipe diameter of 10 cm, the $MgOH^+$ concentration was only reduced from 1 wt.% to 0.975 wt.%.

Based on these results, the annular PFR performance was assessed given its greater ratio of electrode surface to reactor volume. For the annular PFR, the outer diameter and flow rate were varied whereas the length and inner diameter were fixed at 10 m and 10 cm, respectively. The results are shown in Figure 3.4.2-3.

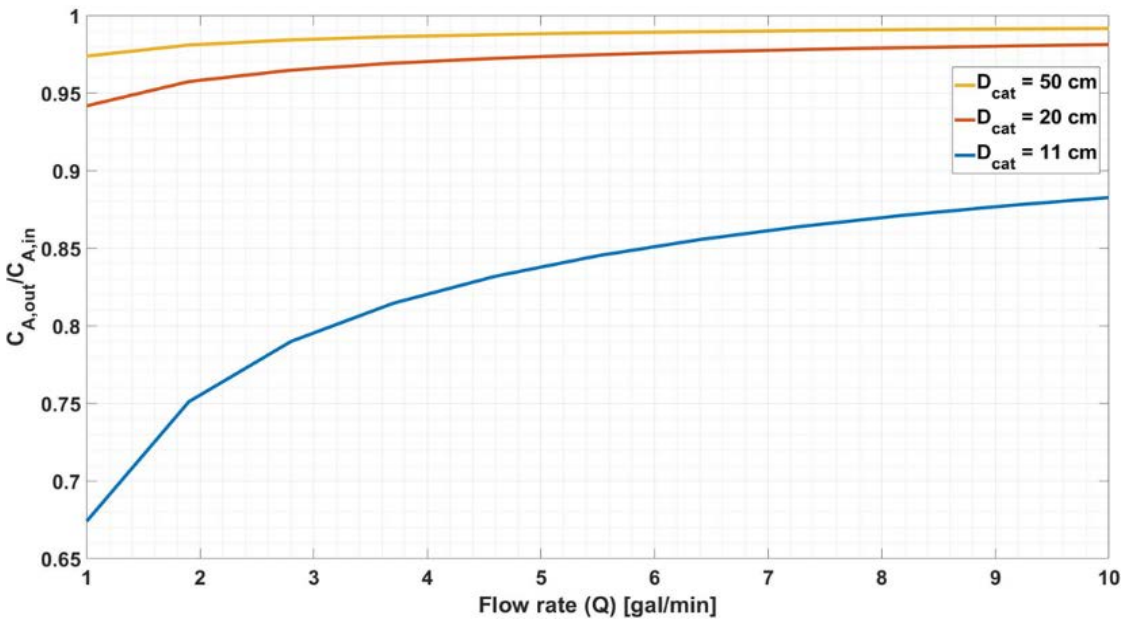

Figure 3.4.2-3. *Annular PFR reactor performance versus outer pipe diameter and flow rate.*

Thus, the reactor performance significantly improves as the outer diameter approaches the inner diameter, i.e., better performance as the two electrode surfaces approach each other. This emphasizes the need for the electrochemical purification cell to optimize the electrode surface area to reactor volume.

To compare all three reactors, we calculated what height/length would be required to achieve a 90% reduction in $MgOH^+$ (i.e., achieving 0.1 wt.% starting from 1 wt.%). The flow rate was fixed at 1 gal/min, the pipe diameters were fixed at 10 cm; for the annular PFR, the inner and outer diameter were 10 cm and 11 cm, respectively. The results are shown in Table 234.2-2.

Table 3.4.2-2. *Reactor height/length required to reach 90% reduction of $MgOH^+$.*

	CSTR	PFR	Annular PFR
Required height/length, m	3462	886	58

The annular PFR shows two orders-of-magnitude improvement over the CSTR. Based on the results, flow rate is critical to the performance of an electrochemical purification process; lower flow rates are desired to increase residence time inside the reactor. Therefore, the expected high flow rates in the molten salt loop (68-110 gallon/min) would be too high. A way to circumvent this problem is to locate the purification unit in a bypass stream or to place units in parallel. These ideas are illustrated in Figure 3.4.2-4.

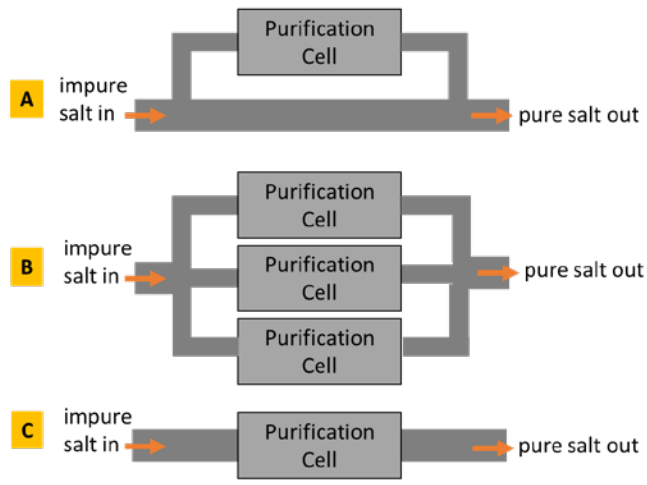

***Figure 3.4.2-4**. Possible configuration for molten salt purification using an electrochemical cell.*

Thus, for the pilot plant, the analysis showed that the pathway depicted in a) and b) are best suited for an online purification unit to lower the inlet flow rate and increase the residence time.

3.4.3. Preliminary Engineering Design

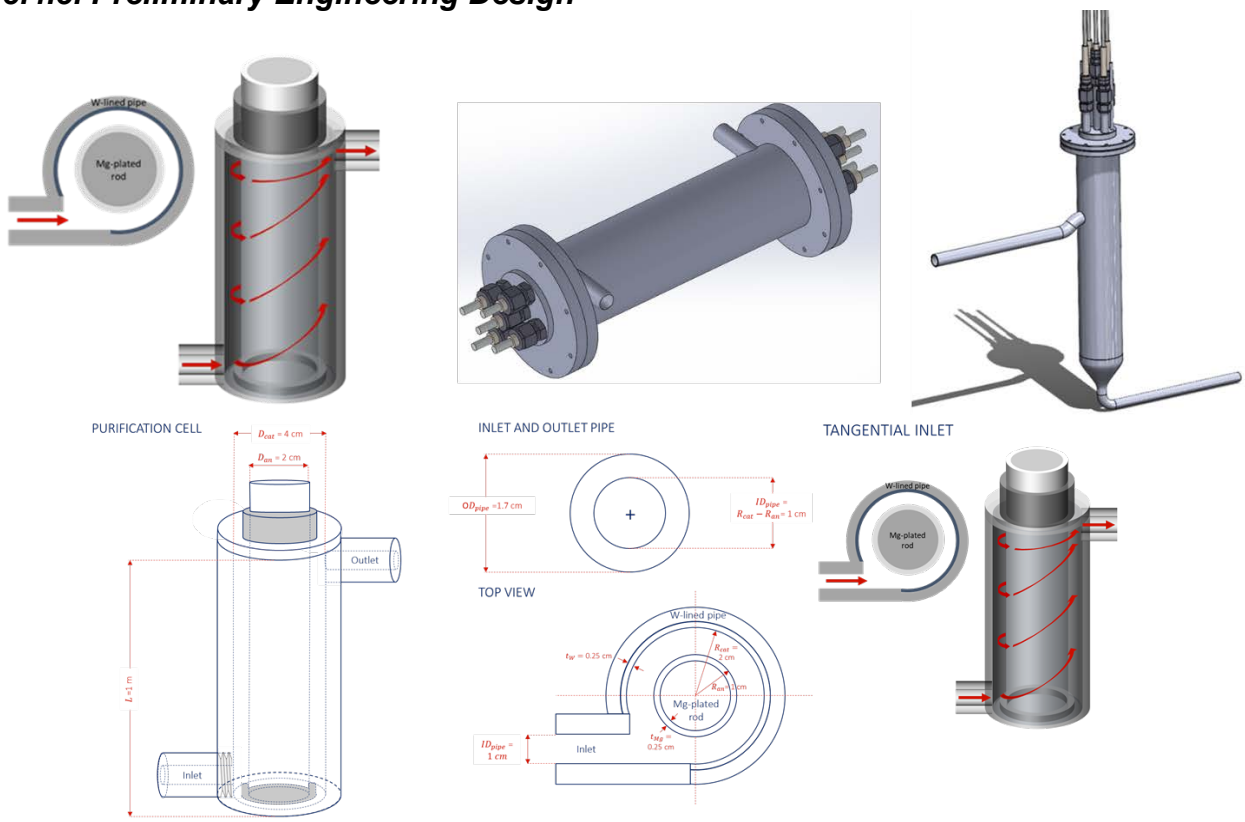

***Figure 3.4.3-1**. Evolution of purification unit design. Original annular reactor top (left), tubular design with electrode inserts, (top middle), and upright tubular design with electrode inserts (top right). Schematic with dimensions (bottom)*

The evolution of the reactor design focused on increasing operability. Originally, an annular design was proposed, which would have the vessel as the cathode with a Mg plated rod insert as the anode. This would require special pipe design at the inlet and outlet to ensure electrical isolation from the rest of the flow system. Furthermore, having only a single anode would require the purification unit to go offline when the anode is replaced. This led to the tubular design with electrodes inserted. The electrodes are electrically isolated from the vessel via ceramic sheaths and Swagelok fittings allow electrodes to be inserted and swapped with ease. However, this design would demand the fittings to be leak tight and resistant to the salt. Therefore, in the final design, the vessel was placed upright. This allowed for a gaseous headspace at the top. The reactor is bottom fed with a weir at the top to ensure constant electrode immersion in the salt. The performance of the final design was estimated, illustrated in Figure 3.4.3-2.

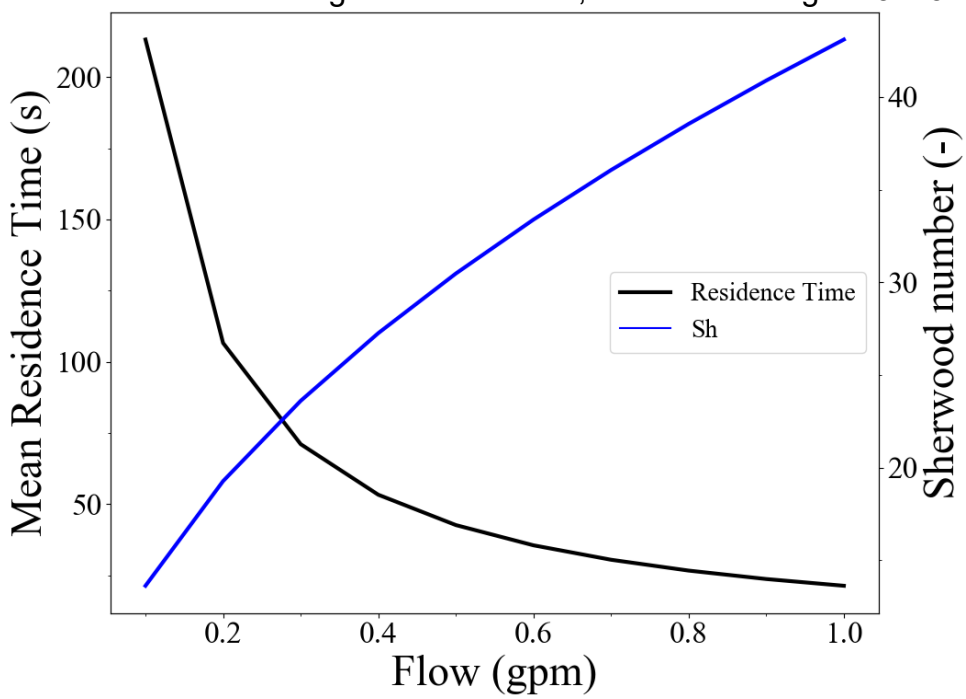

***Figure 3.4.2-2**. Predicted Sherwood number and mean residence number vs. flow rate. From Figure 4, increasing the flow rate from 0.1 to 1 gpm results in the Sherwood number increasing from 14 to 43. While increasing the flow rate enhances the mass transfer of $MgOH^+$, the mean residence time inside the reactor decreases significantly, confirming the previous conclusions from the CSTR and PFR. It is therefore expected that the optimum purification rate will be at lower flow rates.*

3.5. Task 5: Build and evaluate a lab-scale electrochemical purification flow cell to remove corrosive impurities from a flow of ternary MgCl2-KCl-NaCl molten salt.

3.5.1. Task 5 Summary

To support the design of a laboratory-scale flow cell for electrochemical purification, functions governing physics-based scaling relations were established. These scaling relations identified salt flow rate and purification cell geometry as the most important factors governing purification rate. This fulfilled **Milestone 2.5.1.** Based on these scaling relations, a laboratory-scale flow system capable of flowing salt through an electrochemical reactor at a rate of up to 1 gallon per minute was designed, fabricated,

and evaluated in Dr. Mark Anderson's Laboratory at UW Madison (**Figure 3.5.1-1.)**. This system was tested, and purification of MgOHCl was achieved on a much faster timescale than thermal decomposition. Consistent with scaling relations, flow rate and electrode geometry were experimentally identified as the two most important factors governing purification rate. This fulfilled **Milestone 2.5.2.**

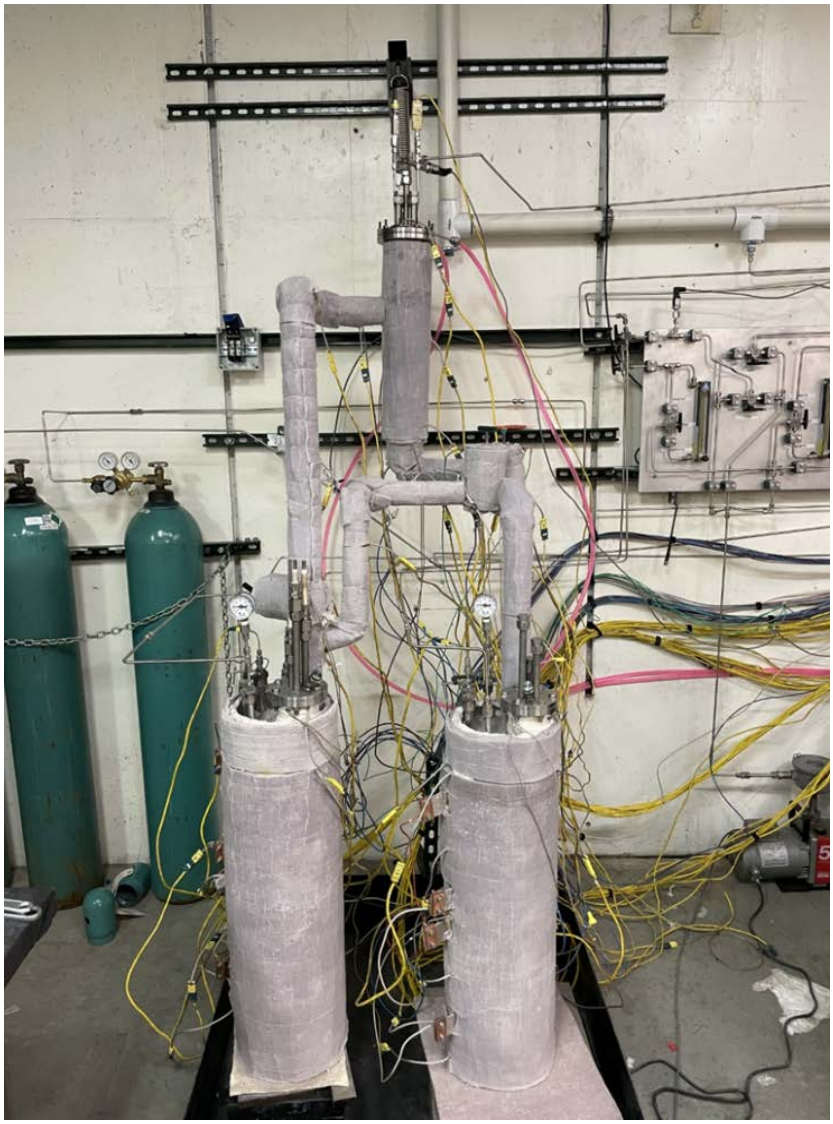

Figure 3.5.1-1*. Completed laboratory-scale flow system for evaluation of electrochemical purification method.*

3.5.2. Design and Safety of Laboratory-Scale Flow Cell

Work in Phase 1 established the optimal reactor design to be one that maximizes the surface area of electrodes to volume of reactor. A final design of the purification reactor based on this concept is shown in Figure 3.5.2-1.

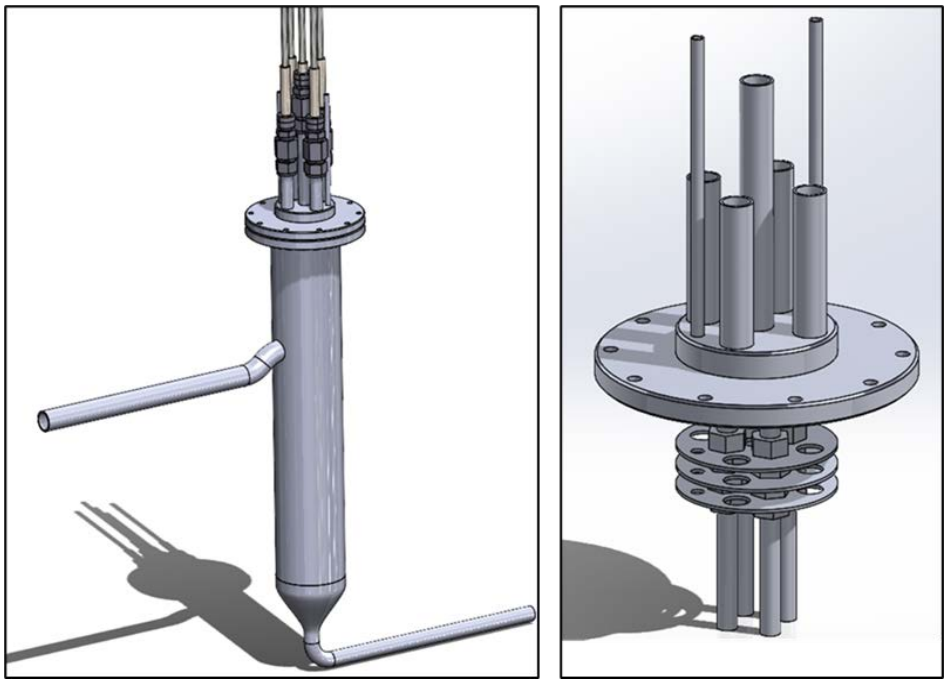

Figure 3.5.2-1. Solidworks rendering of the purification reactor (left), and of the custom lid (right).

The reactor consists of a body built from an 18-in. long, 3-in. schedule 40 pipe and a custom ConFlat (CF) flanged lid; the entire vessel is made from Hastelloy C-276. The reactor is bottom fed with a weir 6 in. from the lid to ensure steady discharge and electrode immersion in the salt. The area ratio of outlet to inlet was designed to be 1.84. The custom CF flange at the top ensures a leak-tight seal while allowing several ports to vary the number of electrodes and configuration. The ports house the electrodes, a thermocouple, and a pressure relief valve to ensure no dangerous amounts of hydrogen will build up in the headspace. Three heat shields are attached to the bottom of the lid with the studs staggered to minimize heat conduction.

The purification reactor was designed to conform to Section VIII of the American Society of Mechanical Engineers – Boiler and Pressure Vessel Code (ASME BPVC-VIII). This was required due to the pressure control system for the flow system exceeding 15 psig. To do so, the pressure rating of several components was calculated. The details of the pressure rating calculations can be found in Appendix B. A summary is provided here.

The cylindrical pressure rating was calculated for the purification vessel body assuming a safety factor of 5, and a weld joint efficiency of 0.5. The maximum allowable pressure was 471 psi. The circular end plate pressure rating was calculated for the reactor flange with the same safety factor and weld joint efficiency. The maximum allowable pressure was 1139 psi. The bolt strength rating was calculated for a bolted flange using stainless steel 316 bolts. The maximum allowable pressure was 991 psi. None of the calculated pressure ratings exceeded the maximum pressure of the flow system of 20 psi.

A thermal stress analysis was also conducted to account for thermal expansion. A finite element analysis was conducted in Solidworks for the purification reactor at 500ºC and 150 psi (Figure 3.5.2-2). The highest stress predicted in the reactor was 119.5 MPa

and therefore was well below the maximum allowable stress of 154 MPa for Hastelloy C-276 at 500ºC.

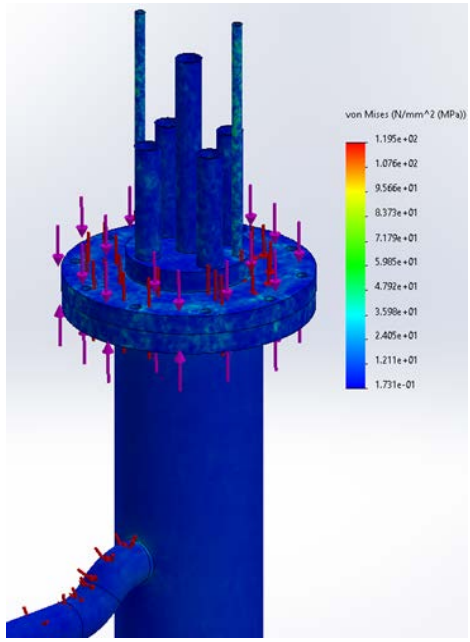

Figure 3.5.2-1. Stress analysis performed in Soldiworks for purification vessel. The highest stress predicted in the reactor was 119.5 MPa and well below the maximum allowable stress of 154 MPa for Hastelloy C-276 at 500ºC.

3.5.3. Laboratory-Scale Flow Cell Fabrication

The Hastelloy C-276 component of the reactor was sourced from Corrosion Materials. These parts and their assembly are depicted in Figures 3.5.3-1-3.5.3-7. The reactor was trace heated and insulated and included several thermocouples as shown in Figure 3.5.3-5. A cooling coil and three heat shields were attached to the custom reactor lid as shown in Figure 3.5.3-6. The electrodes to be used in the purification reactor consist of W or Mg rods in an alumina sheath and castable ceramic. The alumina sheath ensures electrical insulation from the electrodes and the reactor body. The final electrode assemblies for the purification reactor are shown in Figure 3.6.3-7.

***Figure 3.5.3-1**. Components of purification reactor as received.*
The welding of the parts was conducted at the Thermal Hydraulics Laboratory at the University of Wisconsin Madison. Figures 4.1.3.2-2 through 4.1.3.2-4 show the welding process of the parts.

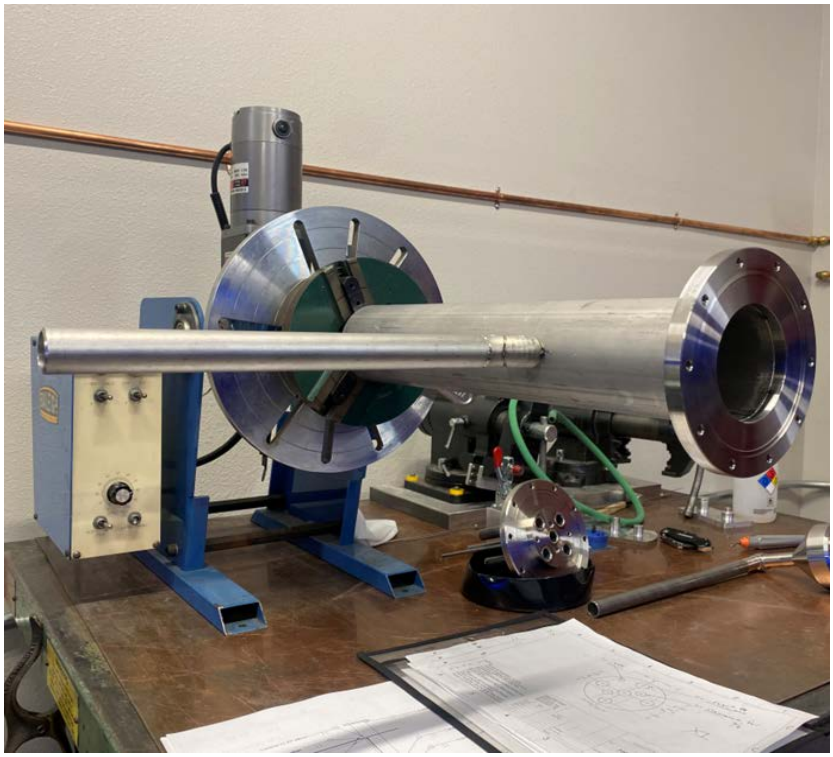

***Figure 3.5.3-2.** Vessel body prepared for welding.*

Figure 3.5.3-3. *Top of purification vessel (top, left and right) and bottom of reactor vessel (bottom).*

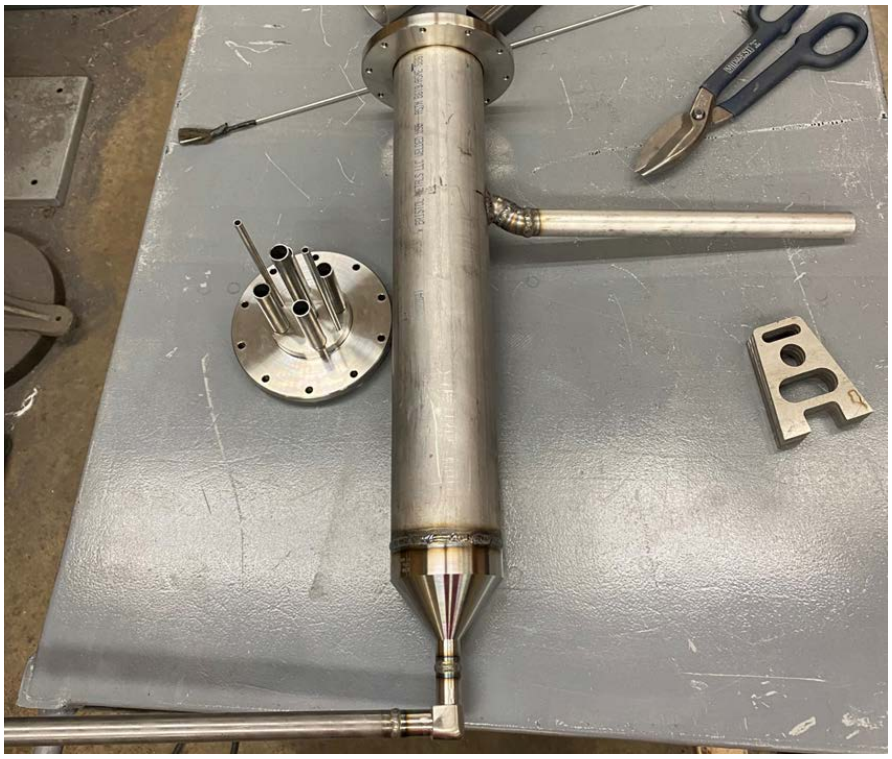

Figure 3.5.3-4. *Completed electrode assembly for purification vessel and salt tanks*.

Figure 3.5.3-5. *Completed electrode assembly for purification vessel and salt tanks.*

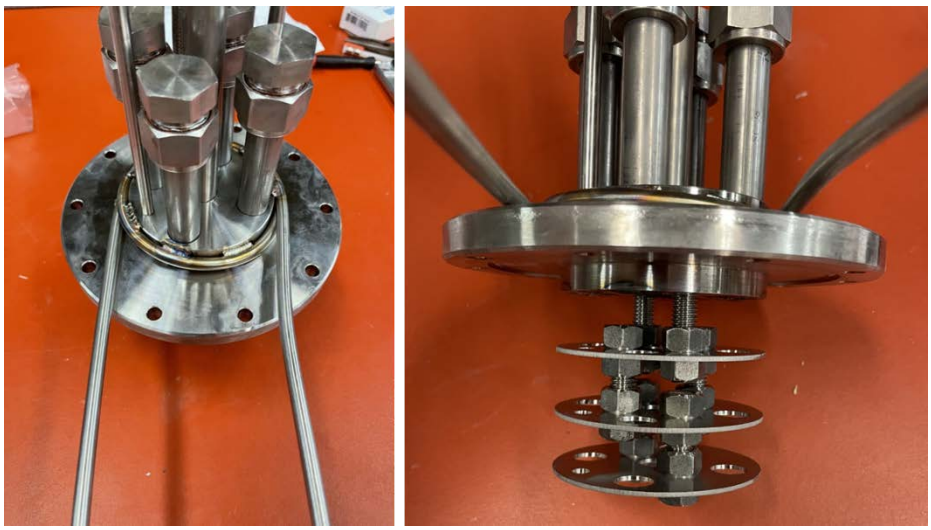

Figure 3.5.3-6. *Completed electrode assembly for purification vessel and salt tanks.*

Figure 3.5.3-7. *Completed electrode assembly for purification vessel and salt tanks. The castable ceramics were heat cured according to supplier specifications*.

Figure 3.5.3-8. *Solidworks rendering of complete flow loop system.*

3.5.4. Laboratory-Scale Flow Cell Operational Experimental Setup

Impurity addition of MgOHCl to the molten salt was done by small additions of NaOH via a two-way valve system installed on the salt containment vessel as shown in Figure 3.5.4-1.

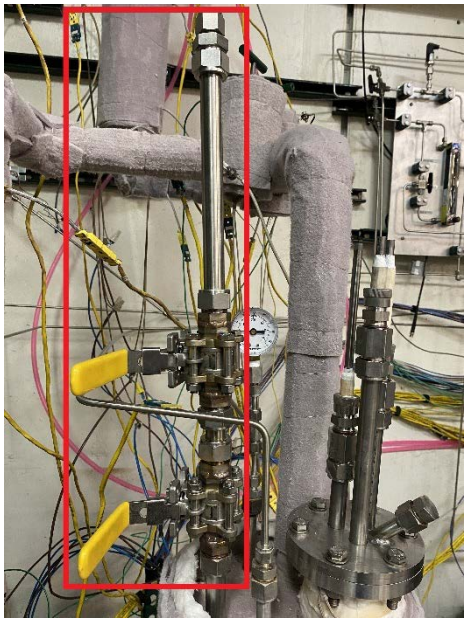

Figure 3.5.4-1*. Two-way valve system installed on vessel #1 for impurity addition.*

The two-way valve system allows for safely introducing impurities into the molten salt without HCl gas evolved from decomposition of MgOHCl leaving the vessel during additions.[1, 19, 23] To avoid excess HCl gas formation, NaOH additions were conducted in batches of 6-8g. We also noticed moisture in the air to make the NaOH pellets sticky and cause clogging in the valves when batches greater than 8g were introduced. After addition of a NaOH batch, the overhead gas flow of N_2 was increased to high flow and N_2 gas was sparged from the transfer line to the bottom of the vessel to create mixing for 10 seconds. A CV was then taken to measure the MgOHCl concentration. A resting period of 5-10 minutes between NaOH batches was implemented to avoid HCl gas exhausting from the valve system during NaOH additions. Batches of NaOH were added until CV measurements indicated impurity concentrations between 2000-2500 ppm (0.2-0.25 wt.%). During experiments we noticed that occasionally the pressure in salt containment vessel #1 rose to 5-10 psig while introducing impurities. This behavior was indicative of the exhaust gas line clogging as shown in Figure 3.5.4-2.

***Figure 3.5.4-2**. Salt condensation clogging exhaust gas line.*

From Figure 4.1.3.5-2, the salt clog occurred at the reducer in the exhaust line. To avoid future gas line clogs the gas line diameter was increased. The installation of the larger diameter exhaust line alleviated the rate at which the exhaust line clogged. We believe that these gas line clogs occurred due to salt condensation from impurity additions. It is likely that the introduction of MgOHCl increases the salt vapor pressure and condenses in the cold section of the exhaust line. This behavior is not exhibited by pure salt, and is noted as an area for further investigation in future related project phases.

To quantify MgOHCl before and after purification experiments CV was employed. A three-electrode system was placed in each of the salt vessels as shown in Figure 3.5.4-3.[25] All electrodes employed for CV were 0.3125” diameter Tungsten (W) rods. To control the surface area of the working electrode a Zirconia based cement was cast around the electrode (Sauereisen #8). When heating the salt vessel for the first time with the electrodes installed, we noticed smoke coming from the exhaust gas line. This was likely due to charring from the organic binder. Therefore, the 2nd working electrode was slowly heated to 500 °C in an oven to remove the organic binder before installment in the salt vessel. Therefore, the working electrode was modified to reduce the amount of Zirconia cement. The modified working electrode used an 18” alumina sheath with the bottom sealed and the top open as shown in Figure 3.5.4-4.

***Figure 3.5.4-3**. Custom flange on receiving salt vessel with electrode setup for CV.*

***Figure 3.5.4-4**. CV electrodes assembly in flange lid of salt vessel.*

The peak current density was used to calculate MgOHCl concentrations after subtracting the background current, as summarized in Table 3.5.4-1.

***Table 3.5.4-1**. Measured and expected MgOHCl concentration after NaOH additions.*

Sum of NaOH added	Measured MgOHCl concentration	Expected MgOHCl concentration
(g)	(ppm)	(ppm)
0	411	411
8.42	730	1129
17.97	1207	1849
43.55	1894	2683

The measured concentration of MgOHCl was lower than the expected concentration based on amount of NaOH added. This behavior was observed throughout all NaOH additions in all 7 experiments. No trend was observed between measured and expected concentrations. A salt sample was taken for analysis via titration and measured $c_{MgOHCl} = 4470 \pm 700\, ppm$. This value was much greater than the measured or expected concentration based on the CV and preparation method. Titration was determined inaccurate due to the method of extracting salt samples, which exposes the molten salt to the atmosphere before sealing in a container.

One potential cause is a large excess of Mg in the salt reacting with the impurity. The concentration would decrease over time if this was the case which was not observed. Three CVs were taken after the last batch of NaOH with five-minute intervals and the results are summarized in Table 3.5.4-2.

***Table 3.5.4-2**. Measured concentration of MgOHCl via repeat CV.*

CV Repeat	Measured Concentration of MgOHCl
-	(ppm)
1	1892.732913
2	1792.482229
3	1894.737927

From CV the measured concentration of MgOHCl stayed consistent after 10 minutes. The concentration of MgOHCl did not decrease across the three CV's as would be expected from excess Mg. Thus, it was determined that likely incomplete stirring of the salt batch before purification caused this issue. Implication of this is an underestimated starting concentration of MgOHCl before purification. This would lead to underreporting the effectiveness of the purification process. For the analysis of the experiments, we used the measured starting concentration of MgOHCl before purification.

During electrode conditioning in salt vessel #2 the scan range was set too high. This resulted in a reducing current of 6A. We noticed afterwards that the signal of the vessel #2 electrodes was suppressed and did not match vessel #1 anymore. It is possible the high currents degraded the working electrode. Therefore, throughout the purification experiments all CVs were conducted in vessel #1.

During salt transfer residual salt remains in each vessel due based on the dip tube height as illustrated in Figure 2. Therefore, throughout experiments the purified salt mixes with

unpurified salt and changes the concentration of MgOHCl. To account for this we measured the total amount of salt transferred between each vessel and the residual salt in each vessel. The total salt transferred between each vessel was consistently measured to be 18.9 kg. It was assumed the remaining salt to be equally distributed in each vessel given their same design. The residual salt in a vessel is then 3.05 kg.

Hall-effect current transducers were employed to measure the current behavior of each individual electrode. The setup of the current transducers and electrical junction box is shown in Figure 3.5.4.-4.

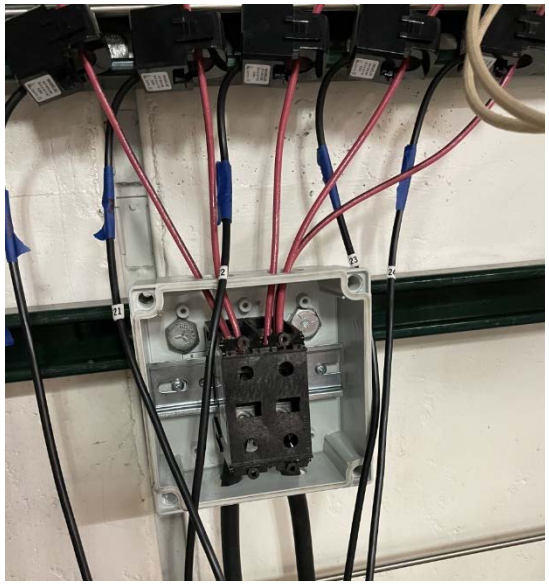

Figure 3.5.4-4. *Electrical junction box and wiring through current transducers.*

This shows the junction box housing all the wiring and a 115A 1-4 power distribution block. The power distribution block allows the positive and negative terminals of the power supply unity (PSU) to be split in parallel to various configurations. Here a 2-3 configuration is shown equal to a 2 cathode – 3 anode setup.

Each individual current transducer was tested for accuracy in a dummy circuit using a 1-ohm resistor. The PSU was set to 10 A and then manually ramped down to 0 A as shown in Figure 3.5.4-5.

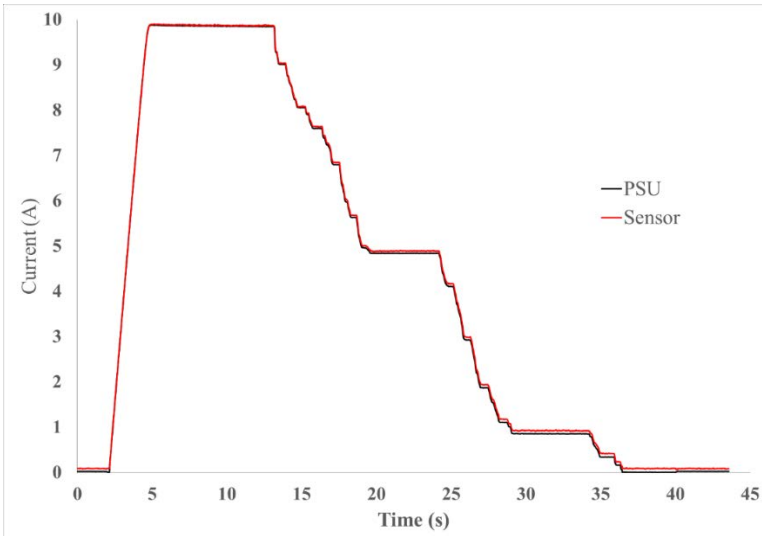

Figure 3.5.4-5. *PSU vs. current transducer reading*.

The current reading from the sensor matched the current profile of the PSU perfectly with time. Only a small offset was detected. Before each experiment, the offset was corrected in the data acquisition module based on the zero current reading. The same test was done to each current transducer to ensure proper function. The results indicate the Hall-effect current transducers are effective in measuring current to each electrode. Finally, Figure 3.5.4-6 shows the LabVIEW program used to control the flow system.

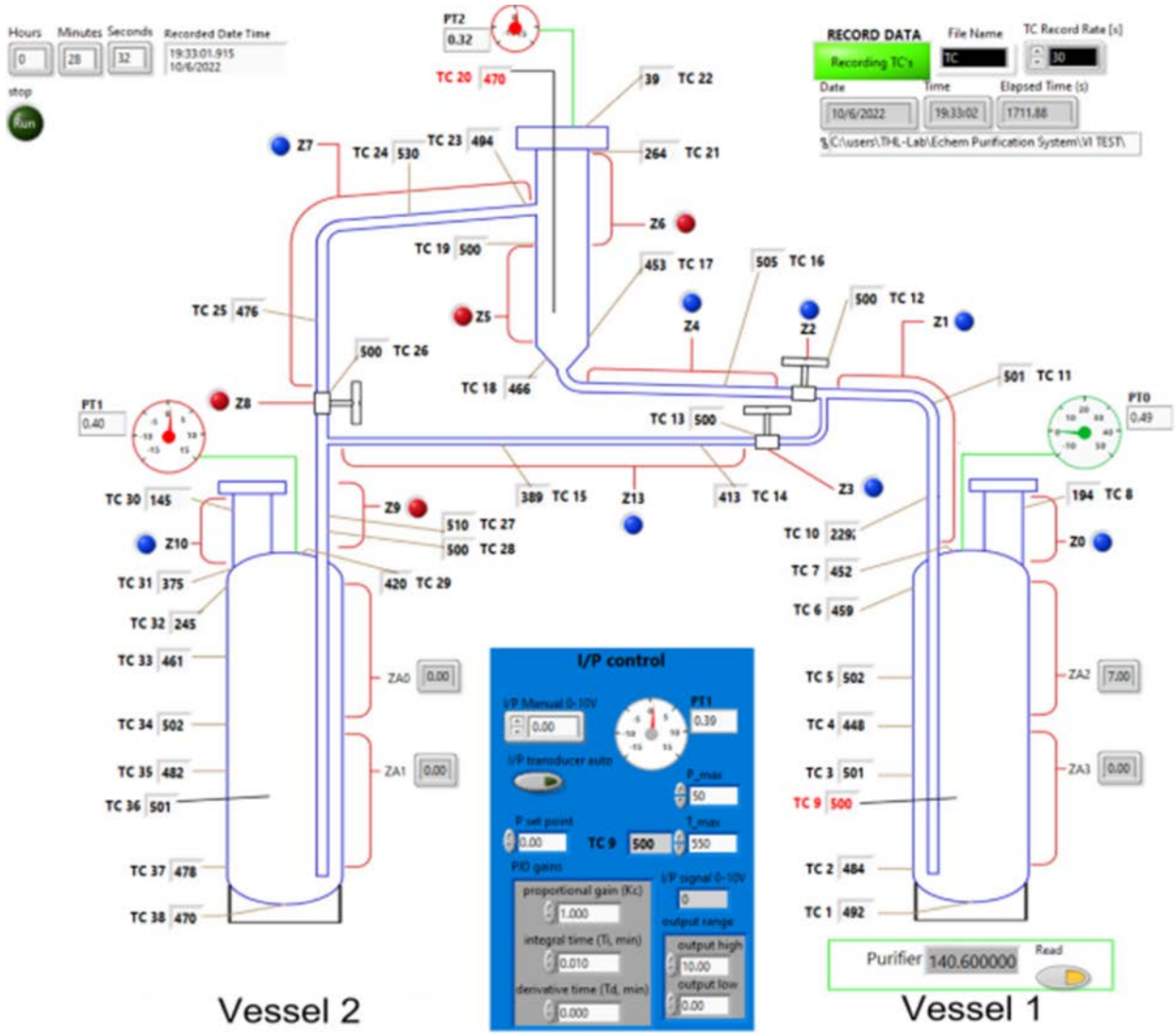

Figure 3.5.4-6. *LabVIEW program used to control flow system.*

3.5.5. Laboratory-Scale Flow Cell Experiments

The first set of experiments (#1-3) evaluated the effect of flow rate using 1-cathode and 1-anode. The electrode configuration is shown in Figure 3.5.5-1. Table 3.5.5-1 summarizes the experimental conditions and results of the flow rate experiments.

Figure 3.5.5-1. *Electrode configuration used for flow experiments #1-3.*

Table 3.5.5-1. *Experimental results of the flow rate experiments.*

Experiment		Flow Rate	Average voltage of Mg vs. W	Average current	Initial concentration of MgOHCl	Final concentration of MgOHCl	Concentration of MgOHCl out of reactor
		(gpm)	(V)	(A)	(ppm)	(ppm)	(ppm)
Low flow (#1)	Run 1	0.096	0.432	5.175	2310	1674	1721
	Run 2	0.062	0.432	5.506	1674	1133	1030
	Run 3	0.097	0.430	5.764	1133	900	863
Medium flow (#2)	Run 1	0.439	0.430	6.102	2400	2412	2669
	Run 2	0.527	0.430	6.216	2412	2308	2298
	Run 3	0.497	0.430	6.187	2308	2238	2242
High flow (#3)	Run 1	0.850	0.431	6.791	1893	2113	2205
	Run 2	0.866	0.431	6.699	2113	2169	2203
	Run 3	0.874	0.431	6.491	2169	2029	2007

The final concentration of MgOHCl reported was after all the salt was transferred back to vessel #1 for CV. The concentration of MgOHCl out of the reactor was calculated after accounting for mixing of the salt in each vessel. The amount of impurity removed decreased as the flow rate increased. This agrees with previous results of a mass transfer limited process; the lower residence time in the reactor leads to lower single-pass impurity removal.

At medium flow rates the amount of impurity removed was minor and at high flow rates the change was undetectable except for run #3. The behavior at high flow rates suggests that the plated Mg on W reached sufficient surface area in run #3 for detectable purification. Furthermore, the final concentration of MgOHCl was higher than the initial concentration for the 1st purification run at medium and high flow rates. This suggests improper mixing of the impurity after doping as discussed previously. Further analysis of the data is presented in Table 3.5.5-2.

Table 3.5.5-2. *Purification reactor metrics from the flow experiments.*

Experiment		Flow Rate	Residence time	Impurity removal rate	Power Consumption
		(gpm)	(s)	(g/s)	(W/g MgOHCl)
Low flow (#1)	Run 1	0.096	234.5	0.047	0.201
	Run 2	0.062	365.7	0.033	0.195
	Run 3	0.097	232.6	0.022	0.486
Medium flow (#2)	Run 1	0.439	51.4	-0.099	-
	Run 2	0.527	42.8	0.050	1.238
	Run 3	0.497	45.4	0.027	2.148
High flow (#3)	Run 1	0.850	26.6	-0.222	-
	Run 2	0.866	26.1	-0.065	-
	Run 3	0.874	25.8	0.119	0.913

The results show that low flow rates are better for single-pass impurity removal. Higher flow rates are better for impurity removal rate at the cost of higher power consumption. Only at low flow rates were we able to reach the target of <1000 ppm MgOHCl, which required three purification passes. The increase in power consumption with flow rate stems from the current behavior. The average current increased with flow rate as shown in Figures 3.5.5-2 to 3.5.5-4.

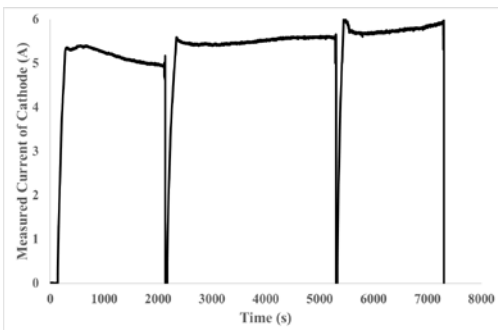

Figure 3.5.5-2. *Current behavior at low flow rates for each purification run.*

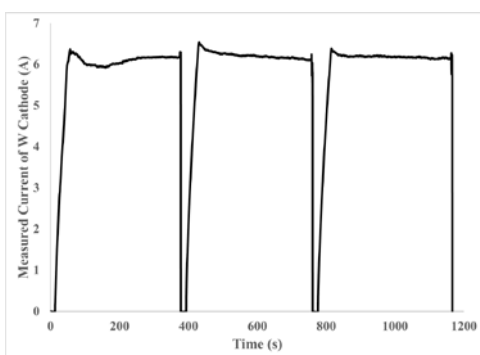

Figure 3.5.5-3. *Current behavior at medium flow rates for each purification run.*

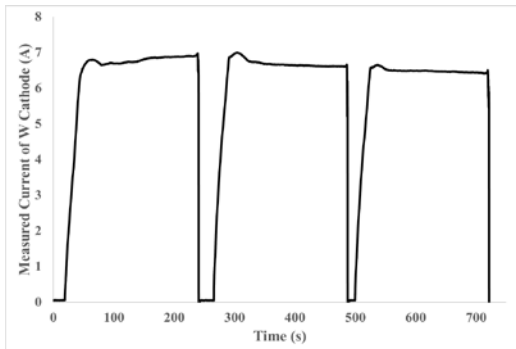

Figure 3.5.5-4. *Current behavior at high flow rates for each purification run.*

The rise in current at the start of each experiment showed the rate at which salt was filling the purification reactor. The current peak at the start of each run was likely the point at which salt started flowing out of the reactor. The current decreased right after the peak and then reached steady state suggesting a period of establishing steady state flow in and out of the reactor. The current behavior after steady state is likely a result of the hydrodynamic behavior inside the reactor. The main trend observed between flow rates was the increase in average current with flow rate.

The purification process never reached the voltage or current limit determined from laboratory batch scale experiments. Throughout all experiments the measured voltage naturally reached a steady value of +0.43 V (Mg vs. W). The results of experiments #1-3 indicated a low flow rate achieved the best single pass conversion. Therefore, the remainder of the experiments were conducted at a flow rate of ~0.1 gpm.

Experiment #4 evaluated the effect of electrode spacing with the configuration shown in Figure 3.5.5-5. Table 3.5.5-3 summarizes the conditions and results of the electrode spacing experiment. Further analysis of the data is presented in Table 3.5.5-4.

Figure 3.5.5-5. *Electrode configuration used for experiment #4.*

Table 3.5.5-3. *Experimental results of the electrode spacing experiments.*

Experiment		Flow Rate	Average voltage of Mg vs. W	Average current	Initial concentration of MgOHCl	Final concentration of MgOHCl	Concentration of MgOHCl out of reactor
		(gpm)	(V)	(A)	(ppm)	(ppm)	(ppm)
Short distance (#1)	Run 1	0.096	0.432	5.175	2310	1674	1721
	Run 2	0.062	0.432	5.506	1674	1133	1030
	Run 3	0.097	0.430	5.764	1133	900	863
Long distance (#4)	Run 1	0.141	0.431	5.822	2388	2224	2285
	Run 2	0.074	0.433	5.779	2224	1355	1138
	Run 3	0.124	0.433	5.843	1355	1201	1199

Table 3.5.5-4. *Purification reactor metrics from electrode spacing experiments.*

Experiment		Flow Rate	Residence time	Impurity removal rate	Power Consumption
		(gpm)	(s)	(g/s)	(W/g MgOHCl)
Short distance (#1)	Run 1	0.096	234.5	0.047	0.201
	Run 2	0.062	365.7	0.033	0.195
	Run 3	0.097	232.6	0.022	0.486
Long distance (#4)	Run 1	0.141	160.2	0.012	1.294
	Run 2	0.074	305.4	0.067	0.122
	Run 3	0.124	182.7	0.016	0.856

The results show that an increase in anode-cathode distance decreased the impurity removal rate and increased the power consumption. Run #2 was an exception, which had the lowest flow rate. Surprisingly, the average currents were higher for experiment #4. It was expected that increasing the distance would decrease the current. The higher current would result in a greater amount of Mg plated onto the W cathode. This would lead to greater impurity removal rates, which were not observed. The data suggests that placement of the W cathode is important for mass transfer of MgOHCl. The W cathode was placed in the center of the reactor for experiment #1 and towards the side of the reactor for experiment #4. As a result, a larger anode-cathode distance was not able to achieve the goal of <1000 ppm MgOHCl after three purification runs.

Experiments #5-7 evaluated the effect of electrode configurations to assess the importance of number of anodes and cathodes. The configurations are shown in Figure 3.5.5-6. Table 3.5.5-5 summarizes the conditions and results of the electrode spacing experiment. Further analysis of the data is presented in Table 3.5.5-6.

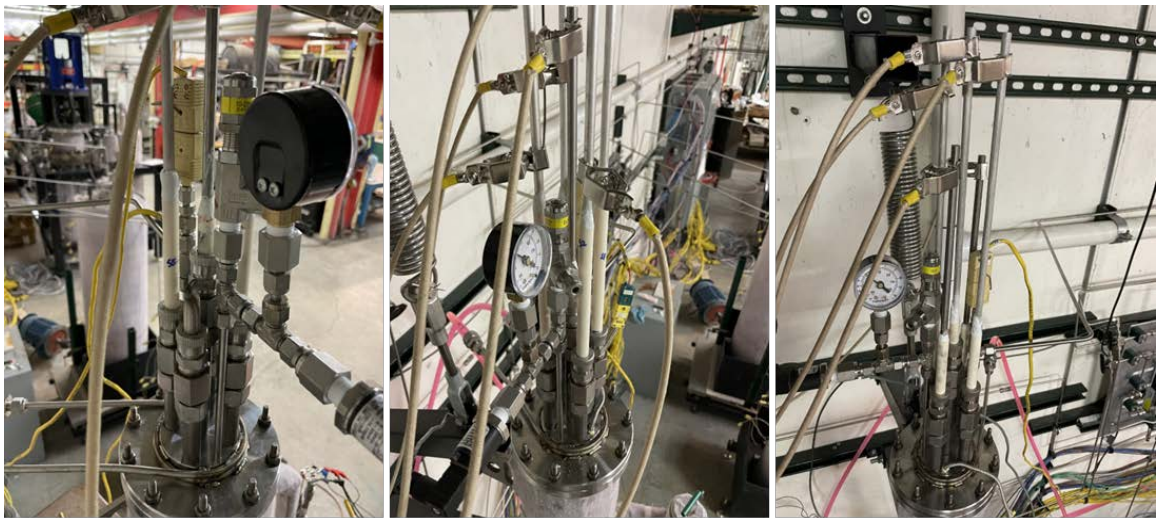

a) Electrode configuration for experiment #5 (1 W, 2 Mg).

b) Electrode configuration for experiment #6 (1 W, 4 Mg).

c) Electrode configuration for experiment #7 (2 W, 3 Mg).

Figure 3.5.5-6. *Electrode configurations of experiments #5-7.*

Table 3.5.5-5. *Experimental results of the electrode configuration experiments.*

Experiment		Flow Rate	Average voltage of Mg vs. W	Average current	Initial concentration of MgOHCl	Final concentration of MgOHCl	Concentration of MgOHCl out of reactor
		(gpm)	(V)	(A)	(ppm)	(ppm)	(ppm)
#5	Run 1	0.121	0.433	11.432	2071	1630	1602
	Run 2	0.094	0.432	11.819	1630	810	583
	Run 3	-	-	-	-	-	-
#6	Run 1	0.098	0.431	13.398	1945	1139	1125
	Run 2	-	-	-	-	-	-
	Run 3	-	-	-	-	-	-
#7	Run 1	0.216	0.430	6.243/6.238	1895	1564	1745
	Run 2	0.249	0.430	6.379/6.346	1564	1069	933
	Run 3	0.034	0.430	6.846/7.143	1069	545	465

Table 3.5.5-6. *Purification reactor metrics from electrode configuration experiments.*

Experiment		Flow Rate	Residence time	Impurity removal rate	Power Consumption
		(gpm)	(s)	(g/s)	(W/g MgOHCl)
#5	Run 1	0.121	184.1	0.048	0.558
	Run 2	0.094	236.8	0.084	0.258
	Run 3	-	-	-	-
#6	Run 1	0.098	222.0	0.070	0.372
	Run 2	-	-	-	-
	Run 3	-	-	-	-
#7	Run 1	0.216	101.2	0.028	1.902
	Run 2	0.249	87.8	0.136	0.459
	Run 3	0.034	642.8	0.018	0.528

Experiments #5-6 did not complete all three purification runs due to a clog in a valve. The transfer lines and valves were heated to 660 °C to attempt to unclog the system from Mg buildup. This method allowed one more purification run to be completed (experiment #6, run #1) before further clogging issues. Experiment #7 was conducted at an earlier date and completed all three purification runs. The average current values for experiment #7 were reported for each W cathode.

Experiment #5 (1 W – 2 Mg electrodes) showed a greater purification rate than experiment #1 (1 W – 1 Mg electrodes). This was likely due to the average current being 2x greater and resulted in more Mg plated onto the W cathode. The removal rate increased by roughly the same factor at the cost of higher power consumption. The increase in average current may indicate that during experiments #1-3 the process was current- limited by the surface area of the anode. This would explain why the expected voltage and current limits were not reached. The configuration of experiment #5 achieved <1000 ppm MgOHCl after just two purification runs. The system clogged after two purification runs of experiment #5. It is likely that the increased current resulted in a less stable Mg film in flowing salt conditions. While purification improves under increased currents, it likely causes more Mg to wash away from the cathode.

Experiment #6 (1 W – 4 Mg electrodes) showed the best removal rate and the highest average current after run #1. The configuration also achieved the highest current observed in all experiments. However, the increase of current from 2 to 4 Mg electrodes was marginal. Surprisingly, the voltage remained steady across all experiments. The voltage and current measured in experiment #6 are likely the natural limit of the Mg reduction process. The current density was calculated to be 0.175 A/cm^2 and serves as the upper bound of the process. Furthermore, the configuration of experiment #6 almost achieved <1000 ppm MgOHCl after a single purification run. The results indicate a higher ratio of anodes to cathodes improves the purification process.

The clog after only one purification run further suggests that higher current causes more Mg to wash away into the salt. Experiment #7 (2 W – 3 Mg electrodes) had the lowest final concentration of MgOHCl after three runs out of all experiments (465 ppm). However,

this experiment was conducted early on when flow rate control was being optimized. Purification run #2 had the best purification metrics out of all runs with an impurity removal rate of 0.136 g/s. Given the single run of experiment #6, it is difficult to determine the best configuration without the aid of simulations or semi-empirical models. Based on the information on flow rate effect, experiment #7 was likely the best configuration. This implies increasing the number of cathodes is more important than the number of anodes. The data from batch experiments further validate this conclusion; it was found that the growing surface area of Mg plated on W was the primary reason for impurity removal.

Analysis of Mg anodes after experiments was also conducted. Diameter measurements were taken along the length of the Mg anodes to assess the rate of Mg consumption. The Mg anodes after the flow experiments. The Mg anode from low flow rate experiments was the most consumed, as expected due to the longer duration of experiments. The consumption of the Mg anode was observed to be random across the length of the electrode.

3.6. Task 6: Mitigate risks associated with MgO buildup. Evaluate risks of formation of H2, including flammability and explosion hazards as well as possible hydrogen embrittlement.

3.6.1. Task 6 Summary

Risks associated with production purification byproducts in the laboratory scale flow cell were evaluated. It was determined that neither MgO nor H_2 posed significant risk in the system as designed, although a slight risk of H_2 pressurization was identified and mitigated.[34] More specifically, in fulfillment of **Milestone 2.6.1**., MgO was evaluated. MgO, which does not adhere to electrodes, was ruled out as a cathodic passivation risk. Furthermore, MgO particles formed during purification were able to pass through a 22-micron filter and were thus ruled out as a clogging risk. It was predicted that MgO formed during purification would settle in the salt holding tanks on an hour timescale. In fulfillment of **Milestone 2.6.2**., H_2 risks were evaluated. The inert gas within the flow system (N_2) mitigated explosion risks. However, a risk of pressure buildup that could be caused by H_2 formation in the event of a clog in the transfer line was identified. This risk was mitigated via use of a pressure relief valve.

3.6.2. MgO Risk Mitigation

Electrowinning experiments were conducted, and a mixture of passivation and mass transfer limited process was observed. This is further detailed in section 3.8, as a part of the kinetics study. MgO film formation on W electrodes was observed but was determined to be only loosely adherent and flaked off throughout repeated electrowinning. Thus, passivation is likely not a concern for this technology, especially under flowing conditions.

3.6.3. H_2 Risk Mitigation

SS316 ¼” tubes were used to fabricate gas lines wo provide controlled flow of UHP N_2 to the system. Vessels 1 & 2 have a gas inlet port and gas outlet port while the purification cell has a gas inlet port and a pressure relief valve as a safety measure against over-pressurization due to production of H_2 gas during purification.

3.7. Task 7: Protect alloys from galvanic corrosion by evaluating down selected materials, avoiding dissimilar junctions where possible and providing engineering solutions, such as use of Mg sacrificial anodes, where needed.

3.7.1. Task 7 Summary

Galvanic corrosion was assessed and a recommended method for future galvanic corrosion assessment was developed, in fulfilment of **Milestone 2.7.1.** While it is possible to determine the rate of corrosion mechanisms individually, it is much harder to know what is happening in a complex final system such as a CSP plant. Our experiments showed that galvanic corrosion cannot be predicted reliably from models, but must be assessed under relevant operational conditions for each galvanic couple identified in CSP plant designs. To enable such evaluation, a protocol for assessment of galvanic corrosion was developed, relying on salt immersion corrosion experiments and electrochemical methods.

To demonstrate this method, the couple of C276 and H230 was evaluated. In contrast to the results that predicted from models of galvanic processes, galvanic contact between the two samples did not significantly increase corrosion. This indicates that, in the sample case of C276 and H230, galvanic corrosion is not the dominant process. Furthermore, immersion of both C276 and H230 in the same salt pot without galvanic contact increased corrosion compared to control experiments with each alloy immersed in its own salt pot. This indicates that the presence of multiple dissimilar alloys in a single molten salt system could accelerate corrosion, even without galvanic contact between the alloys. This may have a significant effect on plant design and performance, and assessment of this phenomenon study is recommended.

3.7.2. Development of Experimental Protocol

We have developed several proposed methods for evaluation of dissimilar materials under consideration for use in an Gen3 CSP system.[3] One of the more useful techniques employs a zero-resistance ammeter (ZRA) to measure the galvanic current between the two samples.[21] By connecting the two metals with a wire that passes through a ZRA, the galvanic current that flows between the alloys can be measured. The measured current can then be used to calculate the corrosion rate. This technique is useful because it only measures the galvanic corrosion in the system, ignoring the effect of other corrosion mechanisms. This allows us to compare the results with the immersion test and start to understand how each other corrosion mechanism contributes to the total.

Another technique that can be used is the potentiodynamic polarization sweep (PPS) or simply potentiodynamic polarization (PDP).[21] PDP is used to measure the corrosion potential (E_{corr}) and corrosion current (I_{corr}) of an electrode in an electrolyte. This is done by first finding the open-circuit potential (OCP) of the material and then sweeping the applied potential from cathodic to anodic polarization while measuring the current density. The resulting polarization curves are used to find the anodic and cathodic Tafel slopes, the intersection of which provide the E_{corr} and I_{corr} of the material. These values can then be used to estimate the corrosion rate of the material in the electrolyte. While this is traditionally a method that predicts the corrosion rate of a single material, superimposing the Tafel plots of two materials, measured separately, allows to find E_{corr} and I_{corr} of the galvanic couple, or E_{couple} and I_{couple}. The point at which the cathodic and anodic potential of the materials intersect represents where the two materials would be polarized to equal potentials if they were coupled. Figure 24 illustrates how the corrosion current is

determined by superimposing the Tafel plots of two separately measured materials. This information can again be used to determine the corrosion rate of the materials in mm/year.

3.8. Task 8: Determine rate of impurity formation in molten salts and rate of thermal decomposition of impurities to HCl to facilitate design for continuous protection throughout the CSP plant.

3.8.1. Task 8 Summary

Milestone 2.8.1 was successfully completed. The rate of MgOHCl formation when exposed to moisture was assessed. Thus, impurity concentration was correlated to moisture ingress, as illustrated in **Figure 3.8.1-1.** This can be used to assess the rate of formation of impurities during Gen3 CSP plant operation, allowing an electrochemical purification cell to be scaled appropriately.

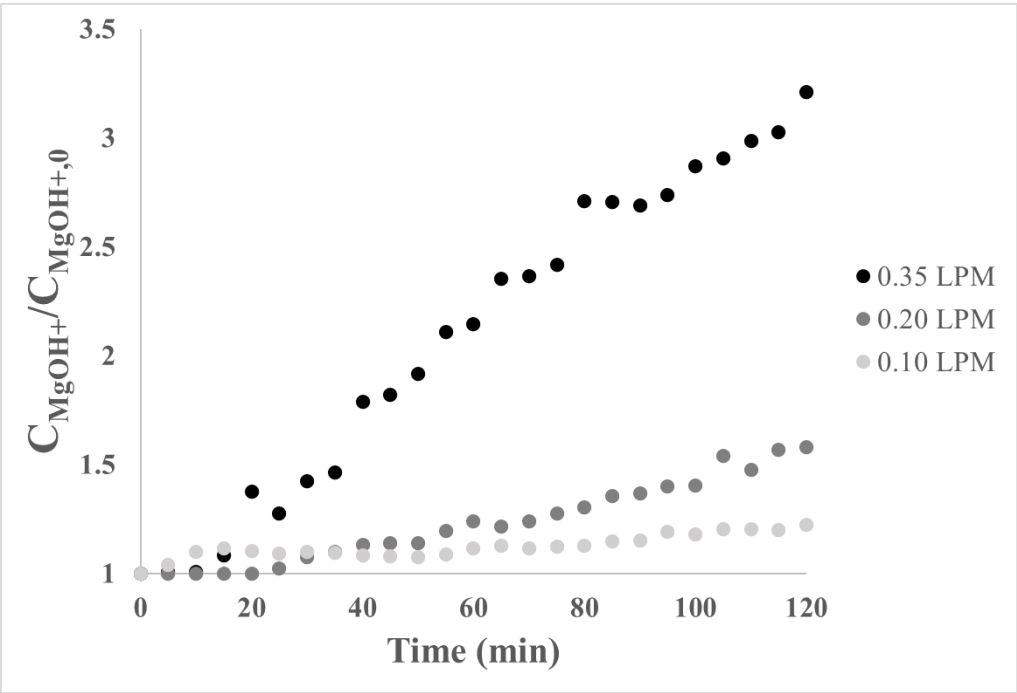

Figure 3.8.1-1. *Concentration of MgOHCl over time in molten salt as a function of inlet gas flow rate with 25 ppm water vapor.*

Furthermore, the rate of MgOHCl thermolysis was assessed, as illustrated in **Figure 3.8.2**. It is important that electrochemical purification proceeds on a faster timescale than thermolysis. Otherwise, thermolysis will occur as a competing process, forming corrosive HCl.

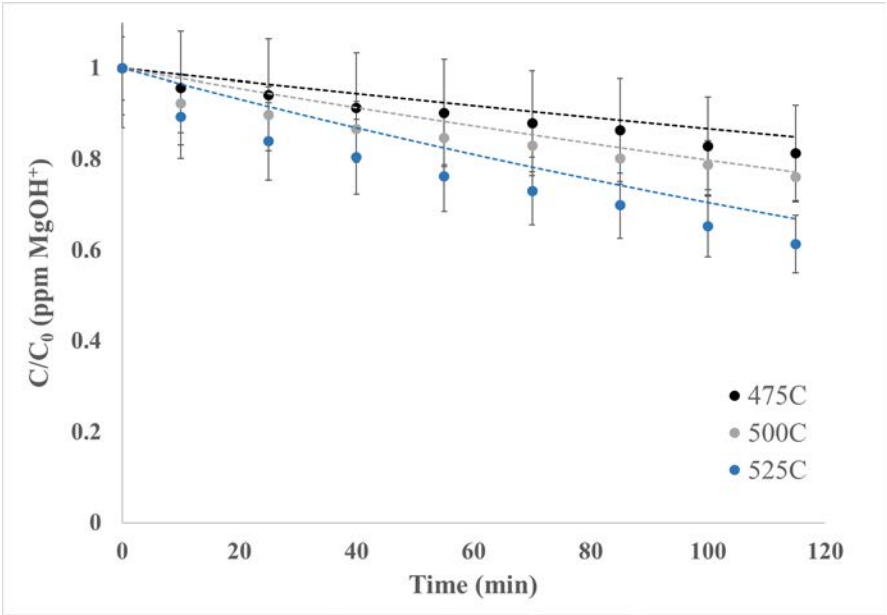

Figure 3.8.1-2. *Experimental concentration of MgOHCl over time compared to values calculated using the Arrhenius expression. MgOHCl concentration reduction is associated with thermal decomposition.*

3.8.2. Assessment of Rate of Impurity Formation, Thermal Decomposition, and Electrochemical Removal

The aim of this work is to obtain key parameters and insight into the mechanism of an electrochemical purification process to aid in scale up and reactor design. We present the electrochemical behavior of MgOH+ reduction on a W cathode in molten MgCl2-KCl-NaCl across the temperature range of 475-525℃. First, the reduction potential of MgOH+ was determined through cyclic voltammetry (CV) and analysis of the electrode surface for MgO via scanning electron microscope (SEM) and energy dispersive spectroscopy (EDS). Second, we present the current behavior of a W cathode through repeated electrowinning and identify the passivation process on W. Based on the current behavior, it is assumed under flowing conditions that the process becomes mass transfer controlled. Last, we present the parameters of reaction, including diffusion coefficient of MgOH+, charge transfer coefficient, standard rate constant, and number of electrons transferred. The results in this study will aid in modeling and scaling a continuous electrochemical purification cell at industrially relevant scales.

A baseline CV of the salt is shown in Figure 3.1.5-1 (0.173 wt.% $MgOH^+$). The chloride salt potential window is bounded by Mg reduction occurring at -1.65V vs. Ag/AgCl and chloride oxidation at +0.2V vs. Ag/AgCl. Four peaks are observed in this window, A-D. Skar also observed peaks A-D using a glassy carbon working electrode. Therefore, the peaks are likely inherent to the species within the molten chloride salt. A consensus on the identity of these peaks has previously not been reached. Both Skar and Guo et al. identified peak B as the reduction of $MgOH^+$. Skar postulated reaction A to be the reduction of hydrogen ions to hydrogen and observed reactions C and D but provided no further discussion on their origin. Guo et al. assumed reaction C to be the oxidation of hydrogen to H^+ and did not provide discussion around peaks A and D. Conversely, Choi et al. and Ding et al. ascribed peak A to be the reduction of $MgOH^+$. Choi et al. also

observed peak D, which they reasoned to be the oxidation of O^{2-}. Ding et al. did not further observe peaks B-D. From this discussion the electrochemistry within Mg-K-Na chloride salt is still indeterminant. To definitively identify the MgOH+ reduction peak, ~1 g of NaOH was added and compared to the baseline CV as shown in Figure 3.8.2-1.

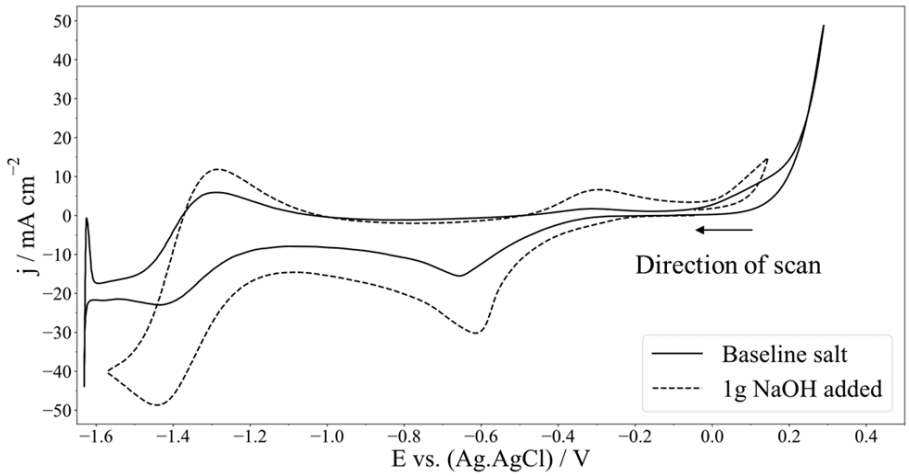

Figure 3.8.2-1. *Cyclic voltammogram obtained on W working electrode in chloride mixture at 500 ℃ and a scan rate of 250 mV/s. Comparison between voltammogram with and without NaOH addition.*

After addition of NaOH, peak current of peaks A-D all increased. This indicates that peaks A-D are all related to an oxide/hydroxide species in the salt. To assess peak A, controlled potential coulometry was conducted for 30 minutes at -0.7V vs. Ag/AgCl. The W working electrode was then slowly raised out of the salt and analyzed as-is under a SEM with EDS. The SEM image is shown in Figure 3.8.2-2.

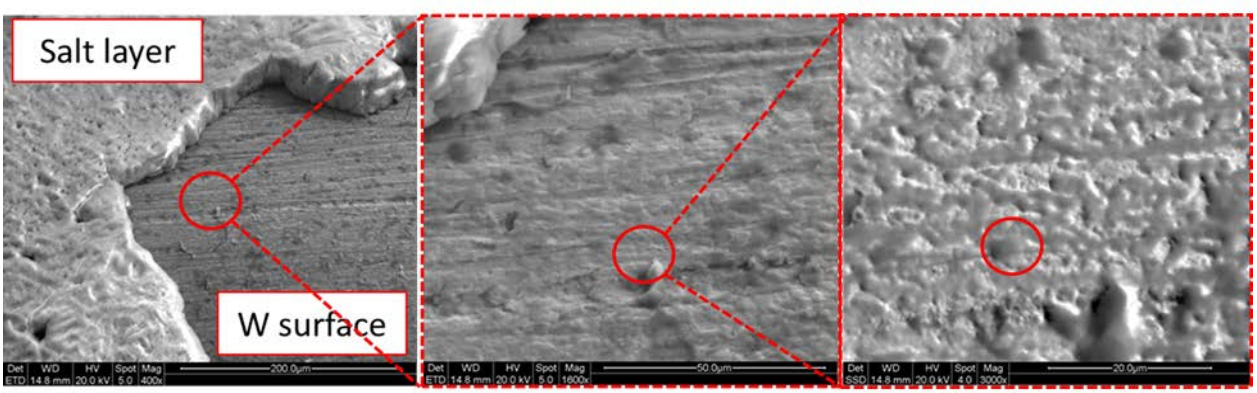

Figure 3.8.2-2. *SEM image of W electrode after 30 minutes of controlled potential coulometry experiment. Left image taken at 400x with a red circle highlighting region of zoom in, middle image at 1600x, and right image at 3000x in backscatter mode*.

By SEM, a thin layer was observed on the W working electrode. EDS point analysis was conducted at the highlighted region (Figure 5.1.1-3, right). Elemental analysis is shown in Figure 3.8.2-3.

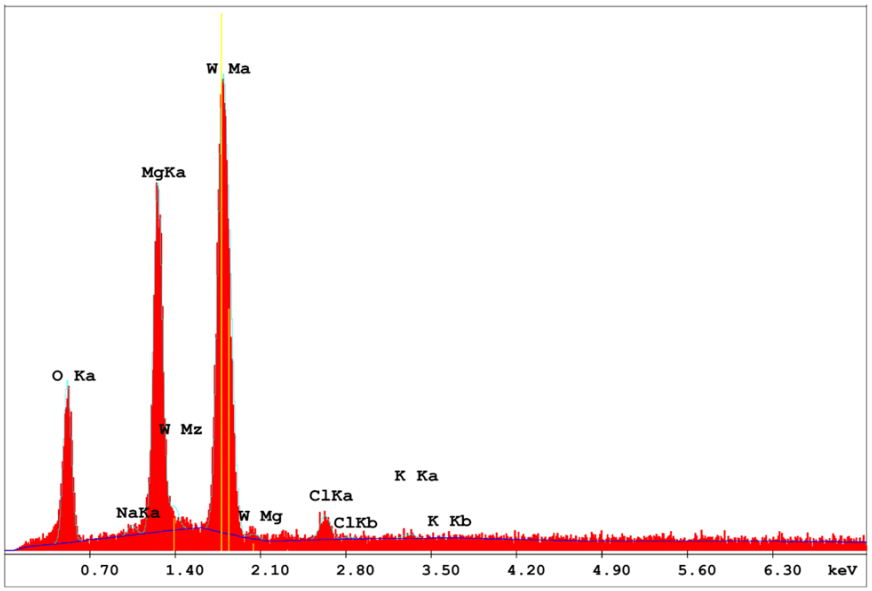

***Figure 3.8.2-3**. EDS point elemental analysis.*

Elemental analysis indicated the plated species consists of primarily Mg (47.6 atomic %) and O (31.09 atomic %) on the W electrode surface (along with salt residue). Given the atomic % values, MgO is the most likely species on the W electrode surface.

With the information from CV and EDS, it is most likely that peak A corresponds to the reduction of MgOH+ according to Reaction (2.3-1). To gain further insight into peaks B-D, voltammograms were taken at various scan rates as shown in Figure 3.8.2-4.

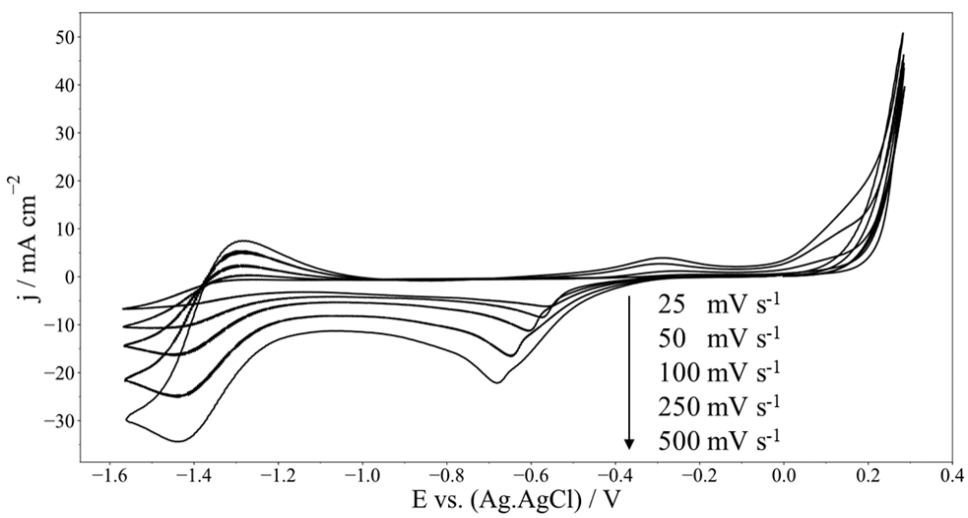

***Figure 3.8.2-4**. Cyclic voltammogram obtained on W working electrode in chloride mixture at 500 ℃ and various scan rates.*

The peak potential of B shifts cathodically with increasing scan rate. This is indicative of a fully irreversible reaction further supporting Reaction (1) with hydrogen bubbling from the electrode surface. Peaks B-C appear to be a reversible one-electron transfer reaction in agreement with the work of Guo et al. The peak current densities of A-D were measured with their background currents subtracted and summarized in Table 3.8.2-1.

Table 3.8.2-1. Current density of peaks A-D at various scan rates.

Scan rate	Peak current density			
($V\ s^{-1}$)	A ($mA\ cm^{-2}$)	B ($mA\ cm^{-2}$)	C ($mA\ cm^{-2}$)	D ($mA\ cm^{-2}$)
0.025	6.06	2.77	1.76	0.20
0.05	8.23	6.65	3.18	0.67
0.1	10.94	10.99	9.29	1.44
0.25	16.01	16.70	15.68	1.91
0.5	21.47	23.02	22.64	1.98
0.75	25.45	31.37	27.07	2.78
1	28.82	36.23	34.12	3.21
2.5	44.83	52.20	53.38	3.65

The current density of peaks B-C match peak A at a 1-1 ratio above a scan rate of 100 mV/s. Peak B is presumed to be a reaction from the product of $MgOH^+$ reduction, either MgO or ½ H_2. MgO is unlikely as the reduction to Mg would be a two-electron transfer reaction. Ito et al. identified the possibility of reducing hydrogen to H^- in molten LiCl-KCl molten salt [69]. The observations make hydrogen reduction the most plausible hypothesis for peaks B-C. Choi et al. mentioned the possibility of O^{2-} involved in peak D. A possible reaction is the oxidation reaction of O^{2-} to form OH^-, with the hydrogen coming from reaction C. To verify, the current density of peak D at 2.5 V/s was calculated with the following assumptions: concentration of O^{2-} of 50 ppm, diffusion coefficient of 1e-5 cm^2/s, and one electron transferred. A current density of 4.37 mA/cm^2 was calculated, close to the measured value. The measured value was lower, probably due to the assumptions in the calculation, or potentially due to the reaction being hydrogen limited. The previous discussion leads to the following set of reactions:

$$Peak\ A: MgOH^+ + e^- \rightarrow MgO + 1/2H_2 \quad [3.8.2\text{-}1]$$

$$Peak\ B: 1/2H_2 + e^- \rightarrow H^- \quad [3.8.2\text{-}2]$$

$$Peak\ C: H^- \rightarrow 1/2H_2 + e^- \quad [3.8.2\text{-}3]$$

$$Peak\ D: O^{2-} + 1/2H_2 \rightarrow OH^- + e^- \quad [3.8.2\text{-}4]$$

With the reduction potential of MgOH+ determined, it is necessary to determine the extent of electrode passivation due to MgO. Ding et al.[7] observed that the current quickly diminished and reached a steady value when electrowinning MgOH+ on a W cathode. The behavior was attributed to W passivation due to MgO. In this work, similar current behavior was observed, as illustrated in Figure 3.8.2.5. To generate this plot, MgOH+ was introduced into the salt by adding ~0.25 g NaOH and then a controlled potential coulometry experiment was conducted at -0.7V vs. Ag/AgCl for 30 minutes while measuring current and cumulative charge transferred.

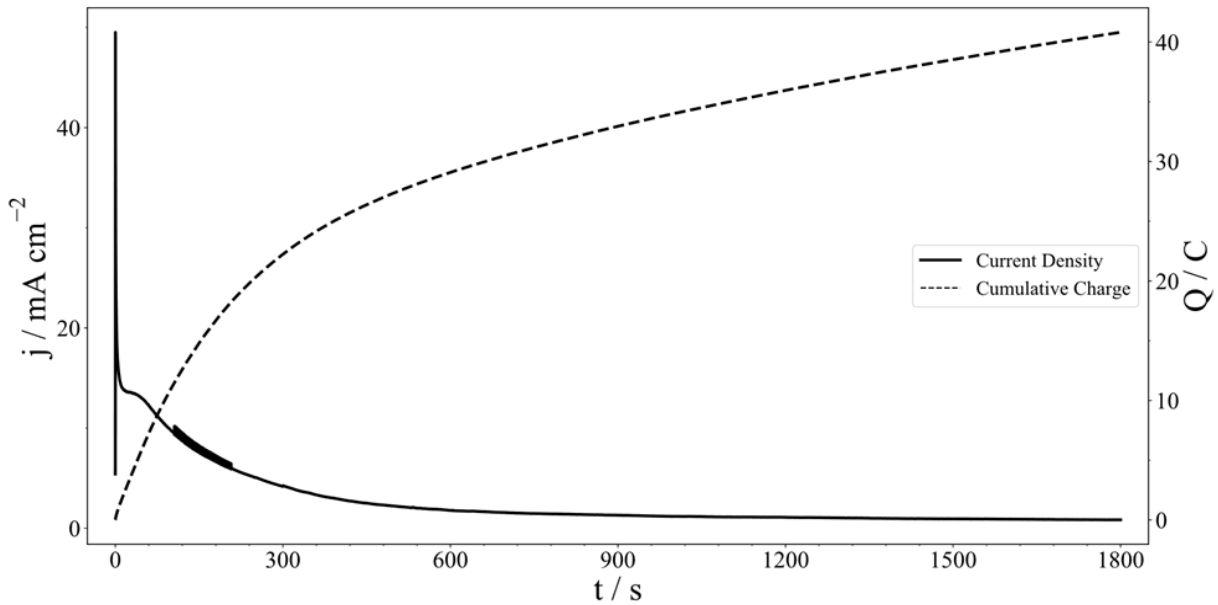

Figure 3.8.2.5. *Current density and cumulative charge vs. time during controlled potential coulometry at -0.7V vs. Ag/AgCl and 500 ℃.*

The current density dropped quickly within the first 5 minutes of the experiment, after which it reached a value of 5 mA/cm2. The current behavior could be due to either passivation or mass transfer limitations. To determine which of these was occurring, 30-minute controlled potential coulometry experiments were repeated for a total of seven times. If passivation occurred, the charge would diminish after consecutive cycles. Between each experiment, ~0.25 g of NaOH was added to ensure each experiment had the same starting concentration of MgOH+. Throughout the cycles the electrodes were not removed or cleaned. The cumulative charge passed in each experiment was normalized to the first experiment (clean electrodes) and shown in Figure 3.8.2-6.

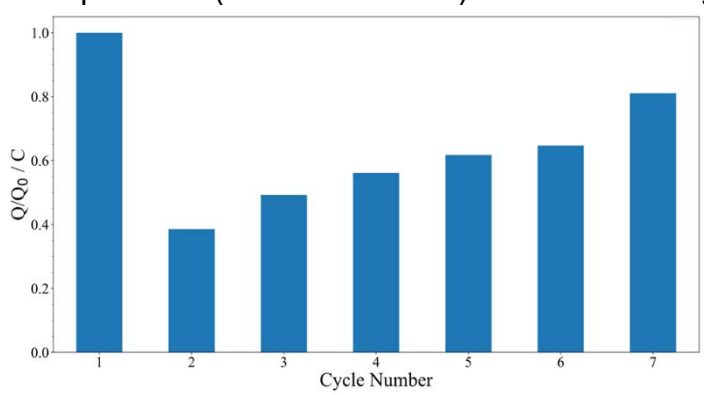

Figure 3.8.2-6. *Cumulative charge passed for each controlled potential coulometry experiment compared to initial experiment.*

Passivation was observed with the total charge passed strongly diminished in the 2nd cycle. However, the charge then recovered in subsequent cycle and reached 80% of the initial charge passed by the 7th cycle. Based on the observed behavior, it is likely that a thin film of MgO is plating the W electrode but is weakly adhered to the W surface. Alternatively, MgO film removal could be attributed to the formation of hydrogen gas

disturbing the film. In either instance, the MgO on the W electrode only partially passivated the electrode upon repeated experiments in a static environment. Under flowing conditions, the MgO film would likely fall off the electrode surface. Alternatively, an electrochemical or mechanical cleaning procedure could be developed for the purification process. Since passivation was not determined to be the primary limiting process, parameters were measured to study the electrochemical purification process under kinetic and diffusion control.

Determination of $MgOH^+$ diffusion coefficient, charge transfer coefficient, and exchange current density via CV was undertaken. Before starting the series of experiments at a given temperature, the bulk concentration of MgOH+ was measured via CV, with the results summarized in Table 3.8.2-2.

Table 3.8.2-2. *Bulk concentration of $MgOH^+$ at each temperature measured via CV.*

Temperature	C^+_{MgOH}
(°C)	(ppm)
475	1751 ± 229
500	1728 ± 120
525	1092 ± 112

The average concentration and standard deviation stem from the CV calibration. The concentration values were used in the remainder of the calculations. So far, the reduction potential of MgOH+ has been identified, and passivation determined to not be controlling the reaction. To determine kinetic versus diffusion control, the following parameters need to be determined: diffusion coefficient of MgOH+, the charge transfer coefficient, standard rate constant, and number of electrons transferred.

To determine the diffusion coefficient of MgOH+ information was used. The peak current density vs. square root of scan rate is shown in Figure 3.8.2-7.

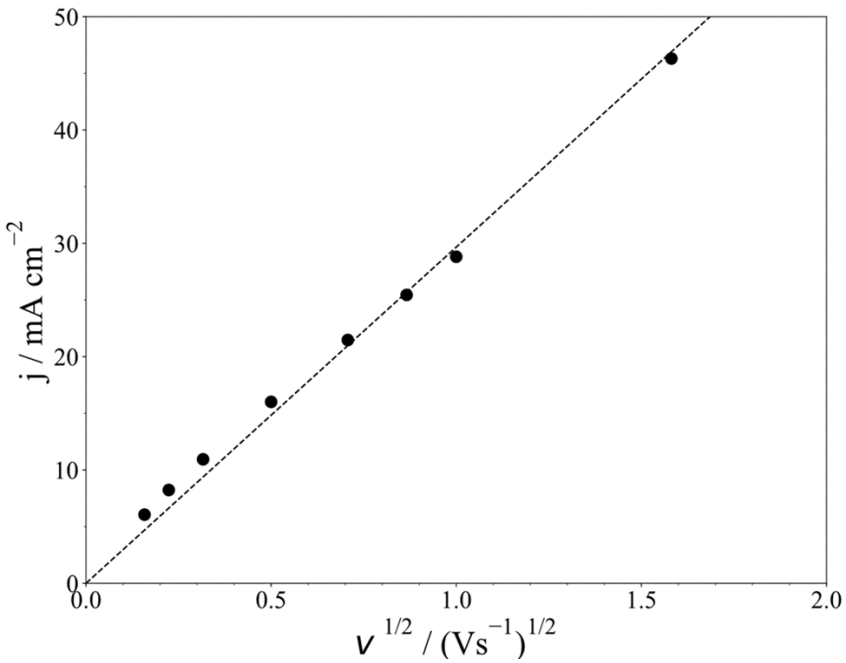

Figure 3.8.2-7. *Peak current density vs. square root of scan rate from 25 mV/s to 50 V/s at 500 ℃.*

This shows a linear relationship through the origin between j_p and $v^{1/2}$ between 25 mV/s and 2.5 V/s, indicating either a fully reversible or fully irreversible reaction. The cathodic shift of E_p with increasing scan rate confirms a fully irreversible reaction. The charge transfer coefficient was calculated to be 0.71 ± 0.02 at 500 ℃. This value for α was used to calculate the diffusion coefficient at 475, 500, and 525 ℃. The diffusion coefficients are summarized in Table 3.8.2-3.

Table 3.8.2-3. *Measured diffusion coefficient of MgOH+ at various temperatures.*

Temperature	Diffusion Coefficient of MgOH+
(℃)	$10^6 \times (cm^2\ s^{-1})$
475	6.839
500	7.334
525	10.090

The measured diffusion coefficients are lower than Skar and close to that of Guo et al. However, the reported values were for hydrogen in peak B-C. Therefore, this work reports for the first time the diffusion coefficient of MgOH+. The diffusion coefficients follow an Arrhenius relationship as shown in Figure 3.8.2-8.

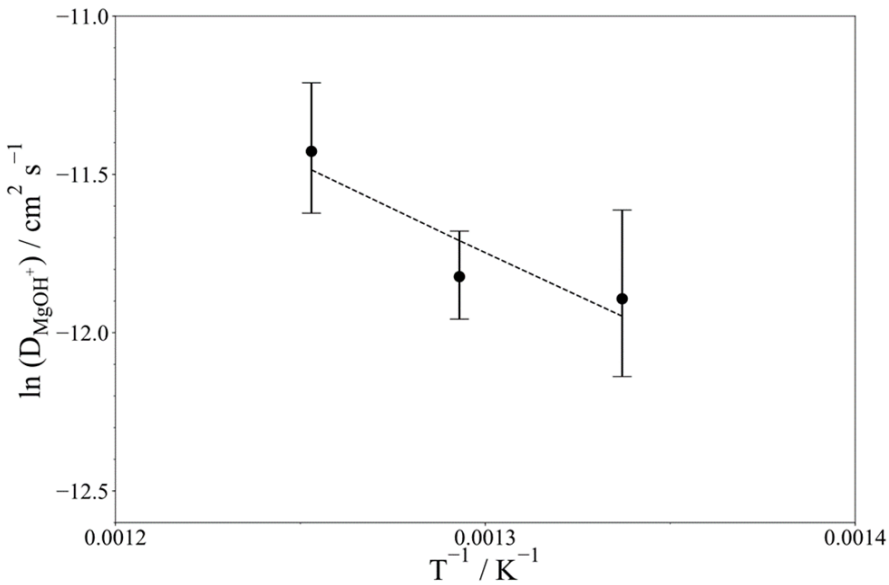

Figure 3.8.2-8. *Arrhenius plot of diffusion coefficient vs. temperature for $MgOH^+$ obtained through cyclic voltammetry.*

The error bars in Figure 3.8.2-7 represent the variance from the concentration measurements from Table 5.1.3-1. The temperature expression of the diffusion coefficient of MgOH+ is presented as:

$$D_{MgOH^+}(T) = 1.034 \times 10^{-2} \cdot \exp\left(\frac{-45{,}880}{RT}\right) \qquad [3.8.2\text{-}5]$$

Before determining diffusion or kinetic control, the standard rate constant k^0 needs to be determined. Therefore, k^0 was calculated at each scan rate. The average and standard deviation is reported in Table 3.8.2-4.

Table 3.8.2-4. *Measured standard rate constant of $MgOH^+$ reduction at various temperatures.*

Temperature	Standard rate constant
(°C)	$10^3 \times$ (cm s^{-1})
475	2.266 ± 0.545
500	2.588 ± 0.702
525	2.691 ± 0.219

The measured standard rate constants of Reaction (2.3-1) follow an Arrhenius relation with temperature as shown in Figure 3.8.2-9.

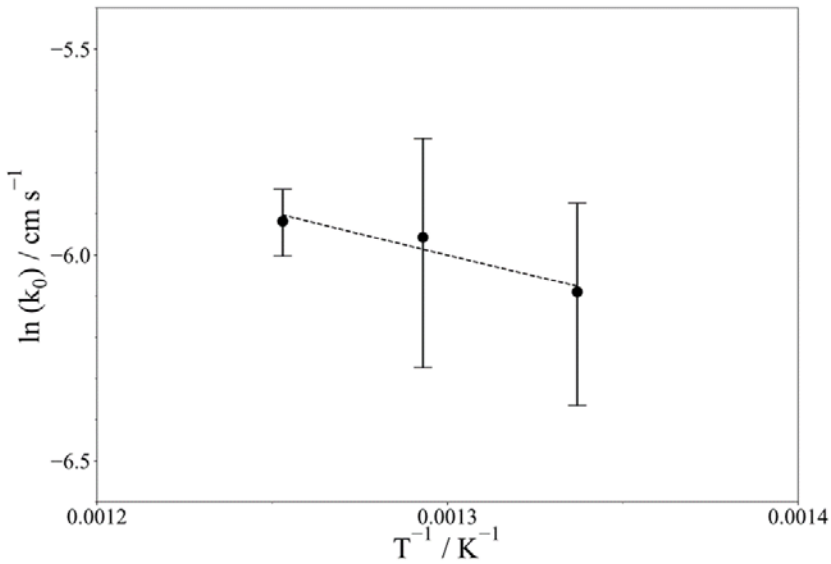

Figure 3.8.2-9. *Arrhenius plot of k^0 vs. temperature.*

An expression for k^0 as a function of temperature was derived as:

$$k^0(T) = 3.625 \times 10^{-2} \cdot \exp\left(\frac{-17{,}157}{RT}\right) \qquad [3.8.2\text{-}6]$$

The standard rate constant is one order of magnitude greater than the reaction of Mg reduction in chloride salts. The relatively low energy of activation barrier, -17 kJ/mol, indicates that the kinetics of the reaction are favorable, and the electrochemical process will most likely be diffusion limited. To confirm, the Damköhler number was calculated and shown in Figure 3.8.2-10.

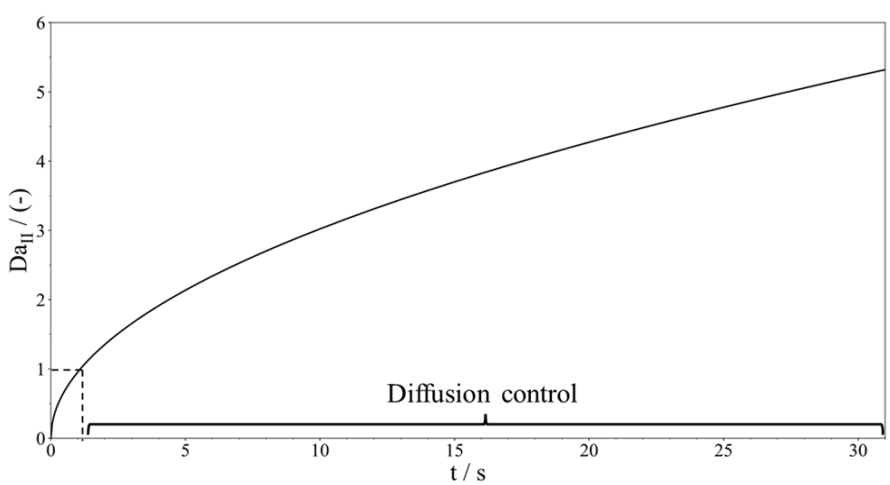

Figure 3.8.2-10. *Damköhler number vs. time.*

This shows that up to 1.1 seconds kinetics control the reaction rate since $Da_{II} < 1$. At 1.1 seconds $Da_{II} = 1$ and the rate of reaction equals the rate of diffusion. This corresponds to a boundary layer thickness of 28.4 μm. After 1.1 seconds the diffusion process takes over due to the growing boundary layer. The boundary layer thickness

is an important factor in designing an electrochemical purification reactor. Here the process was studied in static salt conditions, but in a commercial plant the salt will be in flowing conditions. When designing an electrochemical purification process at scale, the mass transfer of $MgOH^+$ to the electrode surface needs to be considered, i.e., if flow conditions lead to a boundary thickness of <28.4 μm then kinetics need to be considered. Since the diffusion coefficient is an important parameter, CP was conducted to verify the values measured from CV. Chronopotentiograms were recorded between 11 and 12.5 mA and shown in Figure 3.8.2-11.

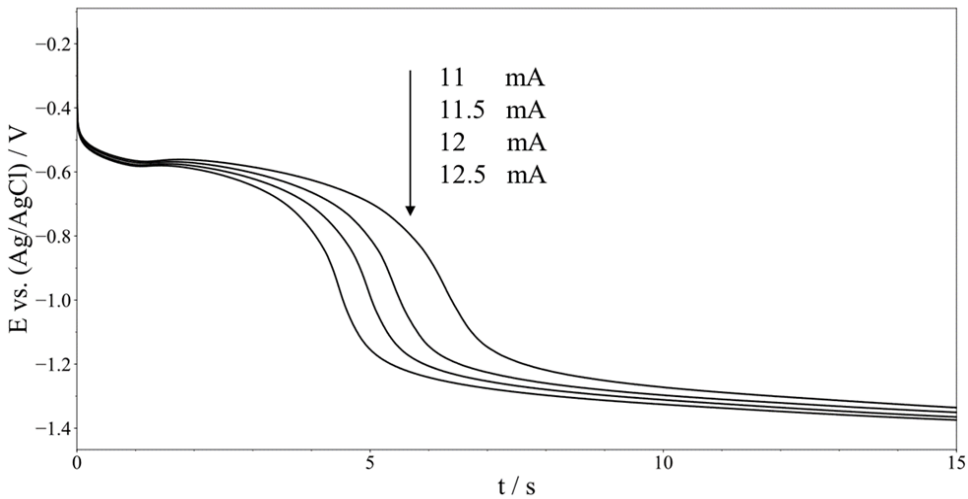

***Figure 3.8.2-11**. Chronopotentiograms at various currents and 500 ℃.*

A plateau is observed at -0.59V vs. Ag/AgCl corresponding to the reduction of MgOH+ as observed in cyclic voltammograms. A second plateau is observed around -1.25V vs. Ag/AgCl corresponding to the 2nd reduction peak observed in the cyclic voltammogram. The decreasing potential of the 2nd potential indicates depletion of ions near the electrode surface. This behavior agrees with the postulation that the 2nd reduction peak corresponds to reduction of hydrogen to hydride ions, and that hydrogen is evolving and slowly bubbling from the electrode surface. The transition times were calculated from and plotted against current densities as shown in Figure 3.8.2-12.

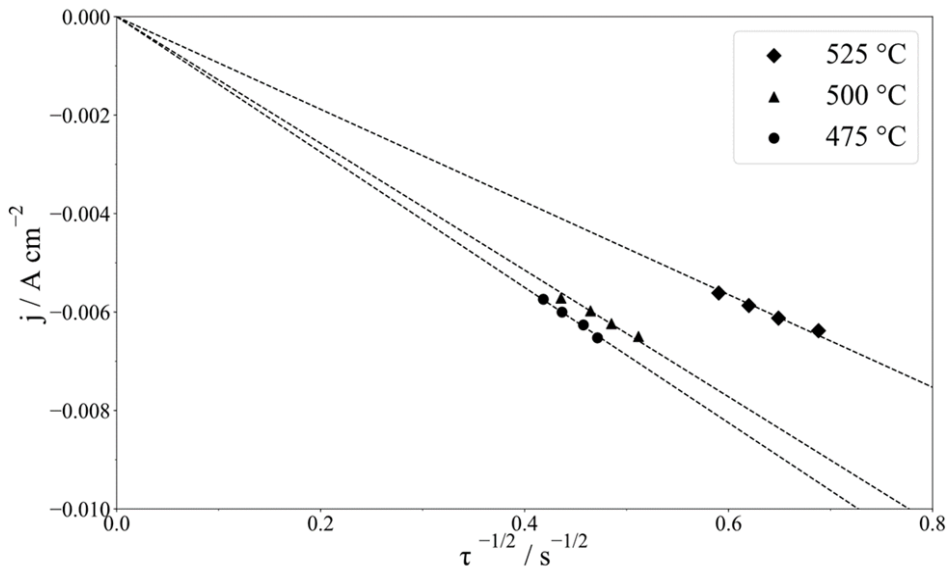

Figure 3.8.2-12*.Current densities vs. square root of transition times at various temperatures.*

The data for all three temperatures showed a linear trend going through the origin, validating the use of Equation (11). The diffusion coefficients obtained are summarized in Table 3.8.2-5.

Table 3.8.2-5. *Measured diffusion coefficient of $MgOH^+$ at various temperatures.*

Temperature	Diffusion Coefficient of MgOH+ (CP)	Diffusion Coefficient of MgOH+ (CV)
(℃)	$10^6 \times (cm^2\ s^{-1})$	$106 \times (cm^2\ s^{-1})$
475	5.030	6.839
500	4.441	7.334
525	6.268	10.090

The diffusion coefficients obtained from CP were slightly lower than those obtained through CV with a discrepancy in the value for 500 ℃. This was likely due to the inherent nature of graphically determining the transition time. Therefore, CV is likely more accurate to determine diffusion coefficients for a fully irreversible process. The diffusion coefficient expression from CP is summarized as:

$$D_{MgOH^+}(T) = 1.444 \times 10^{-4} \cdot \exp\left(\frac{-21{,}338}{RT}\right) \qquad [3.8.2\text{-}6]$$

To verify the number of electrons transferred square wave voltammetry (SWV) was employed. Square wave voltammograms were recorded between 10 and 20 Hz at 500 ℃ and shown in Figure 2.8.2-13.

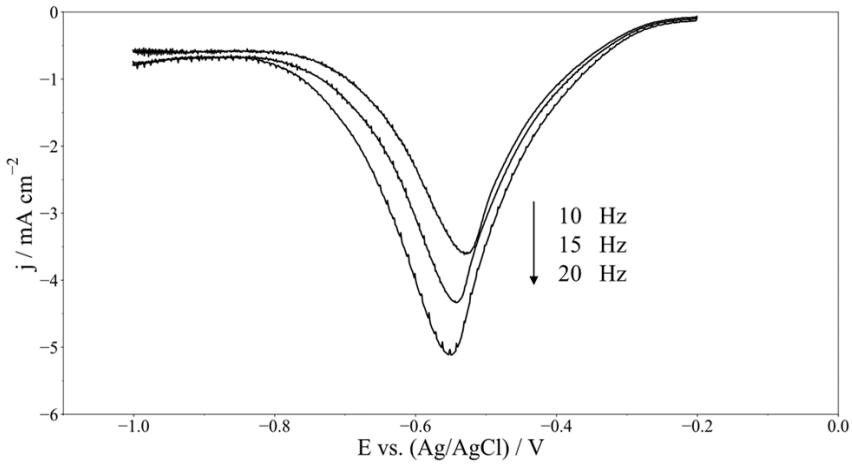

***Figure 2.8.2-13**. Square-wave voltammograms at various frequencies with a step size of 1 mA and pulse size of 25 mV at 500 ℃.*

The square wave voltammograms show a single reduction wave with E_p increasing with frequency. This indicates a single step electron transfer reaction for $MgOH^+$ reduction that is fully irreversible. Using the $E_{p/2}$ obtained at each frequency, and the value of $\alpha = 0.71$ obtained through CV, the value of n was 0.914 ± 0.042, i.e. $n = 1$. This confirms the reduction of $MgOH^+$ as written above. Furthermore, using $n = 1$ and allows α to be calculated, which was 0.65 ± 0.02. This value is slightly lower than 0.71 obtained through CV. The measurements from SWV highlight the utility for irreversible processes in molten chloride salts. With the reaction verified and all the parameters obtained, the current behavior can now be modeled under kinetic or diffusion control.

To verify the parameters obtained in previous sections, the current behavior of the electrochemical purification process was modeled as diffusion controlled the calculated diffusion coefficient was used and the concentration of MgOH+ was 2302 ppm (baseline salt + theoretical amount of MgOH+ added from NaOH). The model is compared to the data in Figure 2.8.2-14.

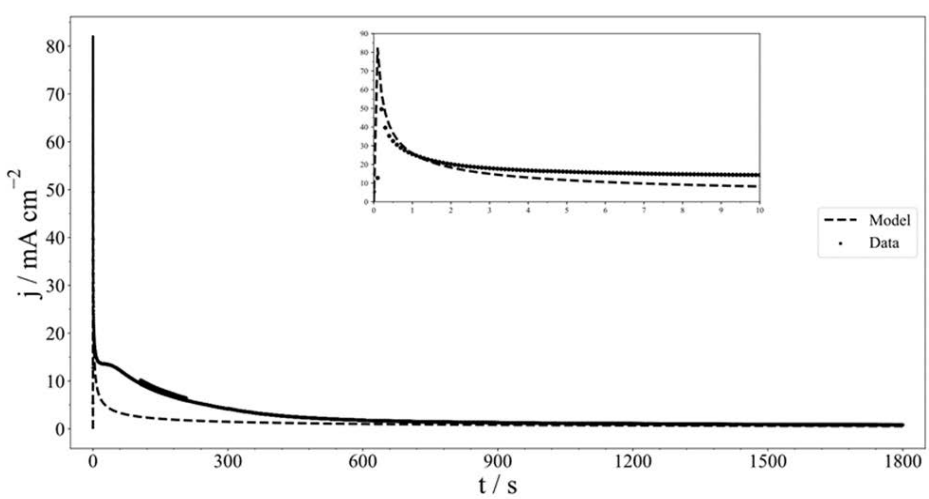

***Figure 2.8.2-14.** Diffusion controlled current modeling compared to controlled potential coulometry experiment at -0.7 V vs. Ag/AgCl and 500 ℃.*

The initial current density in the first 1.1 seconds is lower than the diffusion model. This matches the predicted transition time of the process switching from kinetic to diffusion control. Between 1.1 and 900 seconds the observed current was higher than predicted. This is likely due to hydrogen evolution causing localized stirring of the solution so that the concentration of MgOH+ is higher than predicted. After 900 seconds, the data and model match well, indicating the process is fully diffusion controlled. The results indicate that at long times the limiting current can be modeled. Furthermore, the Damköhler number predicts the behavior of the electrochemical process well. To capture the current behavior between 1.1 and 900 seconds would require knowledge of the hydrodynamics caused by gas evolution.

3.9. Task 9: Package of results into a Tech-transfer document

3.9.1. Task 9 Summary

During this project, new IP was developed, and a provisional patent application was submitted, fulfilling tech-transfer **Milestone 2.9.1.** The new IP consists of a design for the novel 2-electrode method for electrochemical purification developed and evaluated during this project. The 2-electrode setup is more scalable than previously developed 3-electrode methods. The 2-electrode method is based on Magnesium (Mg) electrowinning.

Furthermore, a provisional patent application was submitted for related technology invented under this project. This invention could be used to isolate value-added products from salt using electrochemistry, potentially providing an additional revenue stream and valorizing the purification process.

3.9.2. Patent Application No. 63/480,355

This provisional patent application was prepared during the project and submitted on 01/18/2023. The motivation is described as follows in the application:

Corrosive impurities build up in molten salts. To remove these impurities, electrochemistry may be employed. However, previous attempts to design electrochemical purifications relied on at least three electrodes and did not scale well beyond a laboratory setting. Therefore, there remains a need for a method to remove impurities from molten salts that can scale to industry settings.

4. Significant Accomplishments and Conclusions:

4.1. Summary of Accomplishments and Conclusions

Electrochemical purification is a promising route toward corrosion mitigation in molten chloride salt systems. In this project electrochemical purification was assessed first in bench-scale batch reactor, and then in a laboratory-scale flow reactor. Related phenomena, including galvanic corrosion, thermochemical decomposition of corrosive impurities, and formation of purification byproducts were also assessed. Results of the project indicate that this method is a promising route toward operational control of corrosive impurities in Gen3 CSP plants.

In this report, project tasks and results are described in detail, illustrating that the project milestones were satisfied. More specifically, in Phase 1, a batch reactor was used to assess electrochemical purification, with a focus on reaction kinetics and thermodynamics, as well as form factor of purification byproducts. Galvanic corrosion was also identified as a possible concern. Results of Phase 1 were leveraged to design a

novel 2-electrode purification system, and to produce an engineering design for a laboratory flow cell based on the 2-electrode system. The 2-electrode flow cell system was designed, built, and evaluated in Phase 2. Kinetics and thermodynamics were assessed under flowing conditions, and a protocol for galvanic corrosion assessment and mitigation in Gen3 CSP plants was developed.

The reduction of $MgOH^+$ was determined to be a fully irreversible, one-electron transfer reaction. The electrochemical techniques CV and SWV were utilized to study the reaction. The diffusion coefficient and standard rate constant were determined between 475 and 525 ℃ and temperature-dependent expressions were derived. The charge transfer coefficient of $MgOH^+$ reduction was obtained at 500 ℃. With these parameters the Damköhler number was calculated as a function of time and showed in static conditions the process to be diffusion controlled once the boundary layer thickness exceeded 28.4 μm. The electrowinning process was modeled under diffusion control with close agreement to experiments.

Several focus areas for further research that could accelerate this technology toward industrial deployment have been identified. They include:

- Evaluation of the efficacy of the electrochemical method under turbulent conditions in a larger flow system, such as the FASTR loop
- Development of methods for removal of purification byproducts
- Modeling pilot and industrial scale performance of electrochemical salt purification during plant operation
- Further assessment of the effect of impurities on salt vapor phase.

4.2. Challenges Encountered and Strategies Employed to Address Challenges

The primary logistical hurdle encountered during this research was COVID-related laboratory closures during Phase 1 of this project, and COVID-related supply chain interruption in Phase 2. This resulted in a 1 quarter no-cost extension of Phase 1 of the project, but did not impact the Milestone schedule for Phase 2, and did not compromise or impact project conclusions in any way.

No major technical hurdles were encountered during this project. Several minor setbacks were encountered which caused minor delays and/or small revisions to experimental plans, but none of these impacted overall project objectives.

5. Inventions, Patents, Publications, and Other Results:

As a result of this work, ***two provisional patent applications***, USPTO Application No. 63/480,355 and USPTO Application No. 63/478,806, have been submitted.

One journal article titled “Continuous Purification of Molten Chloride Salt: Electrochemical Behavior of MgOHCl Reduction” has published in the Journal of the Electrochemical Society’s Focus Issue on Molten Salts and Ionic Liquids III[35], and one journal article titled “Predicting and Understanding Corrosion in Molten Chloride Salts” has been published in MRS advances[22].

Additional journal articles are in preparation. One focuses on galvanic corrosion, and has been submitted to Solar Energy Materials and Solar Cells and one focuses on the flow system developed in phase 2. Thus, a total of ***four journal articles*** are anticipated because of this project.

Five conference papers have been published because of this project, including three at SolarPACES (2021 and 2022), one at the 2022 American Solar Energy Society Conference, and one at the American Society of Mechanical Engineers Engineering Sustainability Conference 2021.

Finally, this work has been presented at SolarPACES (2020, 2021, 2022,2023), the 2022 American Solar Energy Society Conference, the American Society of Mechanical Engineers Engineering Sustainability Conference 2021, the 240th meeting of the Electrochemical Society, and the 2022 Annual Meeting and Exhibition, and the ACS 2023 fall meeting, for a total of ***nine presentations*.**

6. Path Forward/Commercialization Plan:

Currently, electrochemical purification of molten chloride salts has been demonstrated in a laboratory-scale flow system capable of achieving a flow of 1 gal/minute. Commercial systems are expected to have flow rates of at least 2-3 orders of magnitude higher.[3, 4] Thus, to achieve commercial viability, this method must be tested at faster flow rates. We recommend intermediate testing in a flow loop such as FASTR or the Villoch loop, which would enable assessment of purification under turbulent conditions without the significant capital investment required to build an industrial scale reactor. Such a project would likely require $500,000 to $1,000,000 in funding and would take 1-2 years. In addition to SunShot, Technology Commercialization Funding could be pursued to support this effort. Furthermore, by including related technologies developed under this proposal (USPTO Application No. 63/478,806), funding sources such as the Advanced Manufacturing Industrial Efficiency and Decarbonization Office may be viable. Finally, engagement with potential customers such as Heliogen has begun. Ultimately, the deployment of this technology would rely on integration with the concentrating solar industry.

References:

1. Zhao, Y.; Vidal, J., Potential scalability of a cost-effective purification method for MgCl2-Containing salts for next-generation concentrating solar power technologies. *Solar Energy Materials and Solar Cells* **2020,** *215*, 110663.
2. Wang, X.; Rincon, J. D.; Li, P.; Zhao, Y.; Vidal, J., Thermophysical Properties Experimentally Tested for NaCl-KCl-MgCl2 Eutectic Molten Salt as a Next-Generation High-Temperature Heat Transfer Fluids in Concentrated Solar Power Systems. *Journal of Solar Energy Engineering* **2021,** *143* (4).
3. Mehos, M.; Turchi, C.; Vidal, J.; Wagner, M.; Ma, Z.; Ho, C.; William Kolb; Andraka, C.; Kruizenga, A. *Concentrating solar power gen3 demonstration roadmap.*; National Renewable Energy Laboratory, 2017.
4. Turchi, C.; Gage, S.; Martinek, J.; Jape, S.; Armijo, K.; Coventry, J.; John Pye; Asselineau, C.-A.; Venn, F.; Logie, W.; Fontalvo, A.; Wang, S.; Robbie; Mcnaughton; Potter, D.; Steinberg, T.; Will, G. *Csp gen3: Liquid-phase pathway to sunshot*; National Renewable Energy Laboratory, 2021.
5. Turchi, C. S.; Heath, G. A. *Molten salt power tower cost model for the system advisor model (sam)*; National Renewable Energy Laboratory 2013.
6. Yan, Y.; Fray, D., Molten salt electrolysis for sustainable metals extraction and materials processing a review. *Electrolysis: Theory, Types and Applications* **2010**.

7. Gong, Q.; Ding, W.; Chai, Y.; Bonk, A.; Steinbrecher, J.; Bauer, T., Chemical Analysis and Electrochemical Monitoring of Extremely Low-Concentration Corrosive Impurity MgOHCl in Molten MgCl2–KCl–NaCl. *Frontiers in Energy Research* **2022,** *10*.
8. Klammer, N.; Engtrakul, C.; Zhao, Y.; Wu, Y.; Vidal, J., Method To Determine MgO and MgOHCl in Chloride Molten Salts. *Analytical Chemistry* **2020,** *92* (5), 3598-3604.
9. Lhermitte, C. R.; Parker, S. S.; Jackson, J. M.; Monreal, M. J., Communication—Mg2+/0 as a Reliable Reference Electrode for Molten Chloride Salts. *Journal of The Electrochemical Society* **2021,** *168* (6), 066501.
10. Hoyt, N. C.; Willit, J. L.; Williamson, M. A., Communication—Quantitative Voltammetric Analysis of High Concentration Actinides in Molten Salts. *Journal of The Electrochemical Society* **2017,** *164* (2), H134.
11. Choi, S.; Orabona, N. E.; Dale, O. R.; Okabe, P.; Inman, C.; Simpson, M. F., Effect of Mg dissolution on cyclic voltammetry and open circuit potentiometry of molten MgCl2–KCl–NaCl candidate heat transfer fluid for concentrating solar power. *Solar Energy Materials and Solar Cells* **2019,** *202*, 110087.
12. Tang, H.; Pesic, B., Electrochemical behavior of LaCl3 and morphology of La deposit on molybdenum substrate in molten LiCl–KCl eutectic salt. *Electrochimica Acta* **2014,** *119*, 120-130.
13. Tylka, M. M.; Willit, J. L.; Prakash, J.; Williamson, M. A., Method Development for Quantitative Analysis of Actinides in Molten Salts. *Journal of The Electrochemical Society* **2015,** *162* (9), H625.
14. Rappleye, D.; Horvath, D.; Wang, Z.; Zhang, C.; Simpson, M. F., Methods for Determining the Working Electrode Interfacial Area for Electroanalytical Measurements of Metal Ions in Molten LiCl-KCl. *ECS Transactions* **2016,** *75* (15), 79.
15. Ding, W.; Gomez-Vidal, J.; Bonk, A.; Bauer, T., Molten chloride salts for next generation CSP plants: Electrolytical salt purification for reducing corrosive impurity level. *Solar Energy Materials and Solar Cells* **2019,** *199*, 8-15.
16. Guo, J.; Hoyt, N.; Williamson, M., Multielectrode array sensors to enable long-duration corrosion monitoring and control of concentrating solar power systems. *Journal of Electroanalytical Chemistry* **2021,** *884*, 115064.
17. Williams, T.; Shum, R.; Rappleye, D., Review—Concentration Measurements In Molten Chloride Salts Using Electrochemical Methods. *Journal of The Electrochemical Society* **2021,** *168* (12), 123510.
18. Ogren, E. Purification and tribology of molten chloride salts. 2022.
19. Mortazavi, A.; Zhao, Y.; Esmaily, M.; Allanore, A.; Vidal, J.; Birbilis, N., High-temperature corrosion of a nickel-based alloy in a molten chloride environment – The effect of thermal and chemical purifications. *Solar Energy Materials and Solar Cells* **2022,** *236*, 111542.
20. Fernández, A. G.; Gomez-Vidal, J.; Oró, E.; Kruizenga, A.; Solé, A.; Cabeza, L. F., Mainstreaming commercial CSP systems: A technology review. *Renewable Energy* **2019,** *140*, 152-176.
21. Gomez-Vidal, J. C.; Tirawat, R., Corrosion of alloys in a chloride molten salt (NaCl-LiCl) for solar thermal technologies. *Solar Energy Materials and Solar Cells* **2016,** *157*, 234-244.
22. Rippy, K.; Witteman, L.; Taylor, P. R.; Vidal, J. C., Predicting and understanding corrosion in molten chloride salts. *MRS Advances* **2023,** *8* (15), 855-859.

23. Zhao, Y.; Klammer, N.; Vidal, J., Purification strategy and effect of impurities on corrosivity of dehydrated carnallite for thermal solar applications. *RSC Advances* **2019,** *9* (71), 41664-41671.
24. Ding, W.; Bonk, A.; Bauer, T., Corrosion behavior of metallic alloys in molten chloride salts for thermal energy storage in concentrated solar power plants: A review. *Frontiers of Chemical Science and Engineering* **2018,** *12* (3), 564-576.
25. Ding, W.; Bonk, A.; Gussone, J.; Bauer, T., Electrochemical measurement of corrosive impurities in molten chlorides for thermal energy storage. *Journal of Energy Storage* **2018,** *15*, 408-414.
26. Villada, C.; Ding, W.; Bonk, A.; Bauer, T., Engineering molten MgCl2–KCl–NaCl salt for high-temperature thermal energy storage: Review on salt properties and corrosion control strategies. *Solar Energy Materials and Solar Cells* **2021,** *232*, 111344.
27. Ding, W.; Shi, H.; Xiu, Y.; Bonk, A.; Weisenburger, A.; Jianu, A.; Bauer, T., Hot corrosion behavior of commercial alloys in thermal energy storage material of molten MgCl2/KCl/NaCl under inert atmosphere. *Solar Energy Materials and Solar Cells* **2018,** *184*, 22-30.
28. Gong, Q.; Shi, H.; Chai, Y.; Yu, R.; Weisenburger, A.; Wang, D.; Bonk, A.; Bauer, T.; Ding, W., Molten chloride salt technology for next-generation CSP plants: Compatibility of Fe-based alloys with purified molten MgCl2-KCl-NaCl salt at 700 °C. *Applied Energy* **2022,** *324*, 119708.
29. Ding, W.; Shi, H.; Jianu, A.; Xiu, Y.; Bonk, A.; Weisenburger, A.; Bauer, T., Molten chloride salts for next generation concentrated solar power plants: Mitigation strategies against corrosion of structural materials. *Solar Energy Materials and Solar Cells* **2019,** *193*, 298-313.
30. Ding, W.; Bonk, A.; Bauer, T., Molten chloride salts for next generation CSP plants: Selection of promising chloride salts & study on corrosion of alloys in molten chloride salts. *AIP Conference Proceedings* **2019,** *2126* (1).
31. D'Souza, B.; Zhuo, W.; Yang, Q.; Leong, A.; Zhang, J., Impurity driven corrosion behavior of HAYNES® 230® alloy in molten chloride Salt. *Corrosion Science* **2021,** *187*, 109483.
32. Gomez-Vidal, J. C.; Morton, E., Castable cements to prevent corrosion of metals in molten salts. *Solar Energy Materials and Solar Cells* **2016,** *153*, 44-51.
33. Gomez-Vidal, J. C.; Fernandez, A. G.; Tirawat, R.; Turchi, C.; Huddleston, W., Corrosion resistance of alumina-forming alloys against molten chlorides for energy production. I: Pre-oxidation treatment and isothermal corrosion tests. *Solar Energy Materials and Solar Cells* **2017,** *166*, 222-233.
34. Glatzmaier, G. *Development of Hydrogen Mitigation for the Nevada Solar One Power Plant*; National Renewable Energy Laboratory, 2020.
35. Witteman, L.; Rippy, K.; Taylor, P.; Vidal, J., Continuous Purification of Molten Chloride Salt: Electrochemical Behavior of MgOHCl Reduction. *Journal of The Electrochemical Society* **2023,** *170* (6), 063502.